Quality Assessment and Improvement on Spark Assisted Chemical Engraving Gravity Feed Micro-drilling

Malek Mousa

A Thesis

in

The Department

of

Mechanical and Industrial Engineering

Presented in Partial Fulfillment of the Requirements
for the Degree of Master of Applied Science (Mechanical Engineering) at
Concordia University
Montreal, Quebec, Canada

August 2008

Your file Votre référence
ISBN: 978-0-494-45315-5
Our file Notre référence
ISBN: 978-0-494-45315-5

ABSTRACT

Quality Assessment and Improvement on Spark Assisted Chemical Engraving Gravity Feed Micro-drilling

Malek Mousa

This thesis presents an investigation on the gravity feed micro-drilling spark assisted chemical engraving (GFMD-SACE). The competitive advantage of the GFMD-SACE process is its combined simplicity and low-cost with high aspect ratio and smooth surface finish. As long as these values are well-preserved and intensified, this process will take a share in the market of micro-fabrication.

The main objective of this study is to establish a systematic approach of the improvement in GFMD-SACE by minimizing initially different variabilities in the process. The methodology is to observe in details the process by adapting the six sigma procedures to determine the major error states and their root causes. To this end, the process initial documentations are created such that it keeps the door wide open for continuous improvement. Based on the initial evaluation, an improved process is recommended on the tool electrode thermal and material properties, electrolyte levels and the use of pulse voltage. Compared to the traditional process, the improvement procedure shows less variability and more capability to achieve high quality in micro-drilling.

ACKNOWLEDGMENTS

There are a number of people without whom this work might not have been completed successfully, and to whom I am greatly indebted.

To my family who have been a source of encouragement and inspiration to me throughout this life. I love you.

I am very also grateful to Dr. Rolf Wüthrich and Dr. Hoi Dick Ng, for their continuous support and non-stopping motivation they created on me.

Special thanks to Mr. Gilles Huard, Mr. Robert Oliver, Mr. Dan Juras, Mr. William Wong and Mr. Henry Szczawinski for helping me building the setups and prototypes for my experiment. Your aid made it less stressful.

To Mrs. Charlene Wald, Dr. Mamoun Medraj and Dr. Brandon Gordon, who encouraged me to change to the thesis option of the master program. Thank you so much.

DEDICATION

To Jerusalem my great home and to my family and friends I dedicate this.

Contents

List of Figures x

List of Tables xiv

List of Symbols xv

Chapter 1 1

Introduction 1

1.1. Statement of problem 2

1.1.1. Process performance 2

1.1.2. Cost of non-quality 2

1.2. Purpose of study 3

Chapter 2 4

Literature and theory 4

2.1. State of the art Spark Assisted Chemical Engraving 4

2.1.1 General overview 4

2.1.2 Gravity-feed micro-drilling 5

2.1.3 Gravity feed micro-drilling sequences and procedure 6

2.1.4 Drilling regimes 7

2.1.5 Viscosity of the machining zone within the hydrodynamic regime 8

2.1.6 Material removal mechanism 8

2.1.7 Chemical etching contribution 9

2.1.8 Heat generation 10

2.1.9 Repeatability of drilling 11

2.1.10 Influence of inter-electrode resistance 12

2.1.11 Machining quality 12

2.2. Quality improvement strategy 15

2.3. Statistical process control 16

2.3.1 Process definition and initial documentation 16

2.3.2 Process variability 17

2.3.3 Quality control tools 18

2.3.4 Process capability 21
2.4. Summary 22
Chapter 3 24
Gravity feed micro-drilling improvement 24
3.1. Potential for improvement 24
3.2. Thesis outline 24
3.2.1 Presenting a strategy for improvement 24
3.2.2 Investigating the heat transfer in the process 25
3.2.3 Investigating the pulse voltage 25
3.2.4 Investigating the electrolyte temperature and level 25
3.2.5 Introducing improvement procedures 26
3.3. Benchmarking 26
3.4. Summary 27
Chapter 4 28
The heat generation in gravity feed micro-drilling 28
4.1. Introduction 28
4.2. Thermal conductivity of tool electrode 29
4.2.1 Experimental procedure 29
4.2.2 Micro-drilling evolution 31
4.2.3 Viscosity of the machining zone within the hydrodynamic regime 34
4.2.4 First seconds of micro-drilling 35
4.3. Applying pulse voltage 37
4.3.1 The goal of using pulse voltage 37
4.3.2 Pulse voltage Circuit 37
4.3.3 Micro-drilling with pulse voltage 39
4.4. Electrolyte level and temperature 41
4.4.1 The importance of electrolyte level 41
4.4.2 Electrolyte circulation and leveling system 41
4.4.3 Micro-drilling with different electrolyte level 42

4.4.4 Need of preheating the electrolyte 44
4.4.5 Electrolyte level adjustment and pulse voltage effect on machining time 45
4.5. Understanding the stair-case-like evolution 46
4.6. Improved process setup 47
4.7. Improving the machining time 48
4.8. Summary 48
Chapter 5 50
Quality evaluation of the process 50
5.1. Introduction 50
5.2. Quality evaluation metrics 51
5.2.1 Mean radius 51
5.2.2 Shape factor 52
5.2.3 Texture 52
5.3. Quality of the traditional gravity feed drilling process 53
5.3.1 Traditional machining conditions 53
5.3.2 Quality at different machining voltages machined during a fixed time 53
5.3.3 Variability of the traditional process 55
5.3.4 Traditional process capability 55
5.4. Quality after improvements 56
5.4.1 Improved machining conditions 56
5.4.2 Quality of micro-holes at fixed depth and variable machining time 56
5.4.3 Quality of machining with pulse voltage without electrolyte adjustment 58
5.4.4 Preheating the tool electrode 59
5.4.5 Preheating the electrolyte 60
5.4.6 Variability of the micro-hole quality with the improved process 61
5.4.7 Capability of the improved process 62
5.5. Quality of machining with tungsten electrodes 63
5.6. Summary 64
Chapter 6 65

Conclusion 65
6.1. Concluding remarks 65
6.2. Recommended improvements for future work 66
6.2.1 To implement electrolyte leveling system 66
6.2.2 To implement tool electrode orbital motion 67
6.2.3 Synchronizing the tool vibration pulse voltage and the dispensing 68
6.2.4 Investigating the overall geometry of the micro-hole 69
6.2.5 Using stair-case-like evolution for predicting quality and machining time 69
6.3. Contribution to knowledge 70
References 71
Appendices 74
Appendix A 75
Appendix B 77
Appendix C 79

List of Figures

Figure 1: Principle of SACE technology: the glass sample to be machined is dipped in an electrolyte solution. A constant DC voltage is applied between the tool and counter-electrode [1]. 4

Figure 2: Evolution versus time plot of four samples of micro-holes performed by gravity feed micro drilling at different machining voltages [3].....5

Figure 3: Sketch of the SACE gravity-feed micro-drilling procedure.....6

Figure 4: Schematic for the initial setup of SACE gravity-feed drilling [4]. The constant force refers to the weight of the drilling head (flexible frame, Top holder and tool spindle with the electrode.....7

Figure 5: Causes of non-predictable machining removal rate in GFMD. 10

Figure 6: Several consecutive glass gravity-feed drillings at 29V with a cylindrical stainless steel tool-cathode of 0.4mm diameter. Applied force was 0.8N. After five successively drilled holes, the evolutions become similar [3].....11

Figure 7: Different micro-hole quality obtained by gravity-feed drilling with a stainless steel 316L tool-electrode of 0.4mm in glass [17].....12

Figure 8: Sample of two micro-holes. Deformed micro-hole because of the tool bending (right) and well-defined circular (left). 13

Figure 9: Evolution of SACE glass gravity-feed drilling in the machining voltage U - drilling depth z plane [3]. 13

Figure 10: Cause and effect diagram of poor micro-hole quality in GFMD. D-D refers to lack of electrolyte at the tip of tool electrode.....15

Figure 11: Step by step approach that is followed in this study [18].....16

Figure 12: A visual summary of Edward Deming approach of variability [19]. 18

Figure 13: Sample of a run charts. Dual run chart of the machining time with the traditional procedures and with the improved procedures.....19

Figure 14: GFMD parameters flowchart. This flow chart is built by the author however all the information included is collected from SACE publications.....20

Figure 15: Process capability plots for different stages of the process.....22

Figure 16: Sketch of the heat transfer in gravity feed micro-machining. The heat is transferred by conduction to the tool electrode (1), by conduction and convection through the electrolyte (2 and 3) and by conduction and convection through the melted zone (4). 28

Figure 17: A sketch for a set of 50 holes at the same sequence of drilling used in the experiment. 29

Figure 18: Typical mean evolution of drilling for 0.5 mm diameter stainless steel(316L), high carbon steel (HCS) tungsten (W) and copper (Cu) electrodes, at various machining voltages (28, 29, 32 and 35 V).....31

Figure 19: Current signals versus time of the electrochemical discharges for stainless steel electrode (316L), high carbon steel (HCS), tungsten (W) and copper (Cu) at 35V.....32

Figure 20: The initial drilling speeds according to the slopes of the fitted curves at the start of the drilling, for 0.5 mm diameter stainless steel (316L), high carbon steel (HCS), tungsten (W) and copper (Cu) electrodes, at various machining voltages.....33

Figure 21: Evolution of drilling depth as a function of time for stainless steel (316L) and tungsten (W) electrodes with a diameter of 0.5 mm, at 28 V machining voltage.....34

Figure 22: Plot of the amplitudes vs. the duration of first seconds of drilling for the last 40 micro-holes, calculated from the real evolution data for stainless steel 316L electrodes, with a diameter of 0.5 mm, at 28 V machining voltage.....35

Figure 23: Typical example of evolution versus time plot for two micro-holes: one machined after preheating the electrode and the other one machined with a tool electrode initially at room temperature. Electrolyte level is 1 mm, electrolyte is initially at room temperature.....36

Figure 24: Pulse voltage, time-on time-off circuit, L=8 mH, R=12.8 Ohms, V=29 V electrolyte 30% wt. NaOH.....37

Figure 25: Current versus time plot for micro-drilling with pulse voltage at various depths. a) At the beginning, b) At depth 25μm and c) At 75μm. RLC values are: L=8 mH, R=12.8 Ohms, V=29 V, electrolyte 30% wt. NaOH.....39

Figure 26: Evolution versus plots of sample micro-drills with pulse voltage (P) and DC voltage (N). The machining voltage is 29 V. The tool electrode is 0.5 mm stainless steel. The electrolyte is preheated to 60C and the electrode is preheated.....40

Figure 27: Schematic of the electrical and mechanical components of the electrolyte circulation system. The heating system is a standalone system consisted of hot plate with built in stirrer and temperature probe.....42

Figure 28: Evolution plots of micro-drilling with high electrolyte level and with low electrolyte level. Machining voltage is 29 V and electrode is stainless steel of 0.5 mm diameter.....44

Figure 29: Evolution plots of two micro-drilling one is drilled with 80°C electrolyte and the other one is drilled without preheating the electrolyte initially. Machining voltage is 29 V and electrode is preheated before the start of the drilling, and it is 0.5 mm diameter stainless steel. The micro-hole depth is 50μm.....45

Figure 30: The effect of manual adjustment of the electrolyte level in reducing the machining time. 46

Figure 31: Stair-case-like evolution that indicates slowdown or stopping in machining (right). Smooth drilling achieved by pulse voltage (left).....47

Figure 32: Comparison between the traditional drilling procedure and the improved procedures. The variability in the machining time is reduced and the mean machining time is minimized.....48

Figure 33: Microscope image of a micro-hole, the vision program tracks the external profile, then ellipse fitting is performed, a is semi-major axis and b is semi-minor axis. (Images are taken by Olympus BX60M microscope with Infinity X digital camera).....50

Figure 34: Well-defined circular contour (left) and full figured deformed micro-hole due to tool bending (right) [17]. 52

Figure 35: Interval plot of mean texture for machining voltages of 28V, 29V, 32V and 35V machined during 60s. 53

Figure 36: Interval plot of linear eccentricity (left) and texture of elliptic shape (right) with the machining voltages at machining voltages of 28V, 29V, 32V, 35V machined during 60s. 54

Figure 37: The quality evaluation of the traditional process. Run charts of shape factor, texture and mean radius for set of 50 micro-holes drilled with the traditional procedures. The condition of the machining is listed in section 5.3.1. The machining voltage is constant 29V DC. 55

Figure 38: Capability plots of the texture and the shape factor for the tradition process. The condition of the machining is listed in section 5.3.1. The machining voltage is constant 29V DC. 56

Figure 39: Shape factor versus machining time for 3 sets of micro-holes machined at different depths. The variability of shape factor increases with increasing the depth. 57

Figure 40: Run chart of drilling time in the case of drilling a micro-hole of fixed depth of 150μm at 29V. The electrode is 0.5mm of tungsten. The tool electrode is not initially preheated, and the electrolyte is preheated to 80 °C. 58

Figure 41: Shape factor versus machining time for two sets of micro-holes machined one with is machined using DC voltage and the other is machined using pulse voltage. The variability of pulse voltage drills is more significant. Drilling depth is 50μm. 59

Figure 42: The effect of preheating the tool electrode. The non-machining duration time is reduced. No significant change in quality is detected. 60

Figure 43: Evolution plots of two micro-drilling one is drilled with 80°C electrolyte and the other one is drilled without preheating the electrolyte (room temperature). Machining voltage is 29 V and electrode is preheated before the start of the drilling, and it is 0.5 mm diameter stainless steel. The micro-hole depth is 50μm. 61

Figure 44: The quality evaluation of the traditional and improved processes. Run charts of shape factor, texture and mean radius for set of 50 micro-holes. Both the traditional and the improved processes use the same setup, however in case of the improved process the electrode and electrolyte is initially preheated, manual adjustment of the electrolyte is performed and the pulse voltage with 29V is used. 62

Figure 45: Capability plots of texture and shape factor for the improved process and the traditional process. Both the traditional and the improved processes use the same setup, however in case of the improved process the electrode and electrolyte is initially preheated, manual adjustment of the electrolyte is performed and the pulse voltage with 29V is used. 63

Figure 46: Two micro-holes, one with less texturing (upper-left) and another one with better shape factor (lower-left) and the corresponding evolution plot of them (right). 64

Figure 47: Schematic of electrolyte levelling technique. 66

Figure 48: Cross-section of electrolyte injecting tool. The electrolyte is dispensed internally to the machining zone to overcome the shortage throughout the drilling. 67

Figure 49: Helical tool electrode, to feed electrolyte into the machining zone to improve the chemical etching and to evacuate the melted material. 68

Figure 50: Sketch of overall control system for GFMD. The vibration, pulse voltage and electrolyte feeding is synchronized. 69

Figure 51: Cause and effect diagram of the process operational cost, if the research and development setup is used as a production setup for GFMD. A-A and B-B are described in figure 5 and figure 10. 75

Figure 52: Pareto diagram of the major error states. The data is collected by an error frequency survey 76

Figure 53: The flow chart of the Micro-hole edge tracking vision system. 77

Figure 54: The output of each step in the vision system 78

Figure 55: The ideal current signal from RL circuit (solid line) and the expected current response when connecting to the machining cell (hidden line) 79

Figure 56: Interpreting the electrolyte level as the interfacing area between the electrode and electrolyte. Iρ is the current density of the cell, and S is the total interfacing area. The tool electrode is 0.5 mm in diameter and the current density is $1.0\ \frac{A}{mm^2}$. 80

List of Tables

Table 1: A quantitative comparison between ultra sonic machining (USM), abrasive jet machining (AJM), laser beam machining, conventional milling and spark assisted chemical engraving (SACE). 26

Table 2: A qualitative comparison between ultra sonic machining (USM), abrasive jet machining (AJM), laser beam machining, conventional milling and spark assisted chemical engraving (SACE). 27

Table 3: Thermal properties of the four tool electrode materials used in this study. 30

List of Symbols

Notation	Interpretation
F	Drag force exerted on the electrode's tip by the melted zone [N]
r	Radius of the spherical object [m]
μ	Molten mixture viscosity [kg/(m. s)]
V	Tool electrode velocity [m/s]
a	Major radius of the fitted ellipse [Pixels]
b	Minor radius of the fitted ellipse [Pixel]
c	Conversion factor
M	Mean radius [μm]
SF	Shape factor [dimensionless]
R_{Tex}	Texture average (roughness) [μm]
R_p	Magnitude of the maximum convex (peak) [μm]
R_v	Magnitude of the maximum concave (valley)[μm]
Cp	Process Capability [dimensionless]
Cpu	Upper Process Capability [dimensionless]
Cpl	Lower Process Capability [dimensionless]
Cpk	Process Capability index [dimensionless]
USL	Upper specification limits [unit of metric]
LSL	Lower specification limits [unit of metric]
σ	Population Standard deviation [unit of metric]
Mean	Population Mean [unit of metric]
S	interfacing surface [μm^2]
r′	radius of electrode [μm]
L	level of the electrolyte [μm]

Chapter 1
Introduction

Spark Assisted Chemical Engraving (SACE) is a non-traditional micro-machining technology based on electrochemical discharges phenomena [1]. It was originally developed for micro-hole drilling in glass by Kurafuji and Suda [2]. SACE uses the heat generated by electrochemical discharges inside a gas film around the tool for locally melting and etching the work-piece. It is a novel machining alternative for fabricating prototypes of micro-fluidic devices, MEMS interfacing and micro-hole drilling. In SACE's Gravity-Feed Micro-Drilling (GFMD), a constant force is applied vertically on the tool electrode. In this case the tool electrode is always in contact with the work-piece. The drilling by gravity-feed is faster compared to the other types of SACE machining, such as constant velocity drilling. On the other hand, the disadvantage of using gravity-feed micro-drilling in SACE machining is the risk of tool bending or breaking, as well as the lack of knowledge about the particular effect of the interacted parameters and their role in forming the quality and the cost of the final product. The heat generation and chemical effect are the two major factors that drive the GFMD process.

SACE gravity-feed micro-drilling has two different regimes in function of the drilling depth: the discharge regime (depths up to 200 to 300 m) and the hydrodynamic regime (depths more than 300 m) [3]. The discharge regime is controlled by the number of discharges taking place in the gas film (by the applied voltage) [3, 4]. Fast drilling (up to about 100 m/s) occurs in this regime. On the other hand, the drilling speed in the hydrodynamic regime is slower (a few m/s), because of the shortage of electrolyte inside the micro-hole during the drilling, limited material removal by chemical etching and the drag force exerted on the tool while penetrating in the molten work-piece [3].

1.1. Statement of problem

Despite that SACE has been known for almost 50 years, the effect of the two major factors of this process is not yet totally elucidated. Those major factors are heat generation and transfer during the micro-drilling and the chemical etching contribution. SACE is distinguished by its simplicity and the ability to fabricate micro-holes with excellent surface qualities without utilizing the expensive clean room facilities. Nevertheless the lack of knowledge of these factors in addition to the non-predictability of machining removal rate and the micro-hole quality obstruct this process from taking a distinctive place in today's micro- machining market. So far, a throughout assessment was not presented and neither a strategy of improvement nor an evaluation technique is available [4].

1.1.1. Process performance

GFMD is characterized by many hardly controllable process parameters such as occurrence of gas film and electrochemical discharges. These parameters can cause variability and make the process unstable and even incapable. Assignable causes, as well as common causes, might combine together to contribute to this variability. The major causes for non-predictable quality and non-predictable machining removal rate are the lack of knowledge about the process, the lack of a real time sensing signal, excess heat at the machining zone and shortage of electrolyte in the machining zone to perform the etching. Some examples of non-desirable micro-hole quality characteristics are heat affected zone, jagged surface and surfaces with cracks. Too long machining times are not desirable. Insufficient material removal rate during the machining is a direct cause for increase of the machining time. Low material removal rate might be caused by the shortage of electrolyte that reaches the melted zone and performs the required etching. This is noticeable mainly during the hydrodynamic regime (depth >100 μm)[6]. Long machining time yields to bad quality micro-holes.

1.1.2. Cost of non-quality

The technology of GFMD is not well established, due to the lack of knowledge of all the parameters - inputs and outputs -, the lack of technology to monitor or control all those parameters and the lack

of knowledge about the significance of each parameter. All the significant parameters in GFMD should be identified and well controlled or their non-desirable effects should be eliminated or at least minimized. The delay in launching this technology (GFMD) might cost this process lost opportunities for the competitor processes. On the other hand, Appendix A.1 investigates primarily the increase of the cost of GFMD in case the research and development setup is used for industrial production.

1.2. Purpose of study

The purpose of this study is to investigate the effect of the main parameters of GFMD on the product quality, the processing time and the behaviour of the drilling evolution. The initial documentation of the process is created in order to start the continuous improvement procedures. The statistical control tools are used to evaluate both the effect of the process parameters and the proposed improvements. This thesis introduces an explicit identification of the GFMD process and a strategy for quality improvement for the first time in the history of SACE and GFMD in particular. This identification places GFMD in the first step of the improvement procedures [4]. The parameter diagram, cause and effect diagrams and pareto diagram are used to find the major error states. Then suggested improvement procedures are then introduced to minimize the variability in both the quality and machining time. Quality evaluation metrics measured by an image processing system is offered. Run charts and capability studies are used to evaluate the improvement in micromachining with GFMD.

This accomplishment is not only necessary for improving GFMD to place itself in the competitive market of micro-machining, but it also can be scaled to benefit similar SACE fabrication techniques, with minimum changes.

Chapter 2
Literature and theory

2.1. State of the art Spark Assisted Chemical Engraving

2.1.1 General overview

Spark Assisted Chemical Engraving (SACE) is a non-traditional micro-machining technology based on electrochemical discharges phenomena [1]. It was originally developed for micro-hole drilling, in glass, by Kurafuji and Suda [2]. SACE uses the heat generated by electrochemical discharges inside a gas film around the tool for locally melting the work-piece. It is a novel machining alternative for prototype fabricating of micro-fluidic devices, MEMS interfacing and micro-hole drilling. Schematics of the SACE set-up is shown in figure 1. Two electrodes, dipped into an electrolyte are supplied by a constant DC voltage. The cathode, with the smallest surface, is used as tool to machine the work-piece [1]. SACE is based on electrochemical discharges which happen through a gas film built around the tool-electrode. Material removal is believed to occur by a combination of thermal and chemical effects. The exact mechanism is still under discussion in literature.

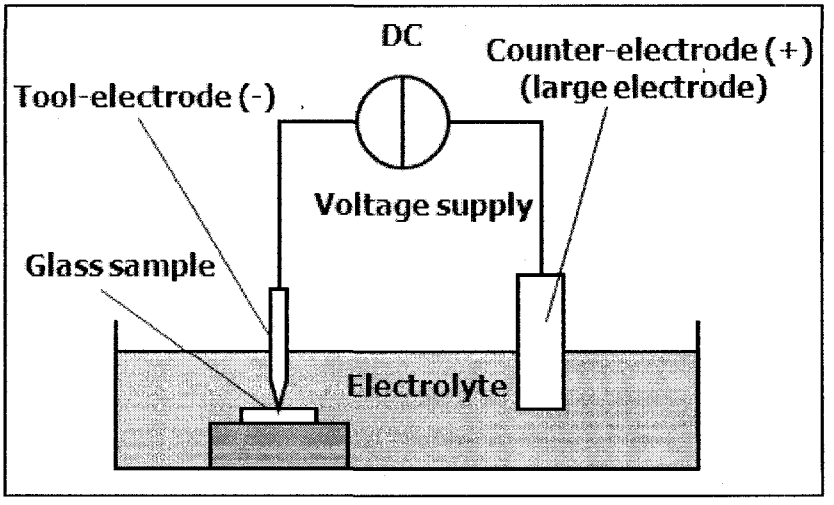

Figure 1: Principle of SACE technology: the glass sample to be machined is dipped in an electrolyte solution. A constant DC voltage is applied between the tool and counter-electrode [1].

2.1.2 Gravity-feed micro-drilling

Gravity-feed micro-drilling (GFMD) is one of the machining techniques used in SACE. In this technique a constant force is applied vertically on the tool electrode. In this case the tool electrode is always in contact with the work-piece. Micro-drilling by gravity-feed is faster compared to the other types of SACE machining, such as constant velocity micro-drilling. On the other hand, the disadvantage of using the gravity-feed micro-drilling in SACE machining is the risk of tool bending or breaking of the work-piece. As during gravity-feed drilling the tool-electrode is constantly in contact with the work-piece, drilling can be followed by measuring the progress of the tool-electrode. Typical examples for glass drilling in function of various machining voltages are shown on figure 2. Drilling was done with a 0.4mm cylindrical stainless steel cathode in 30%wt NaOH [3].

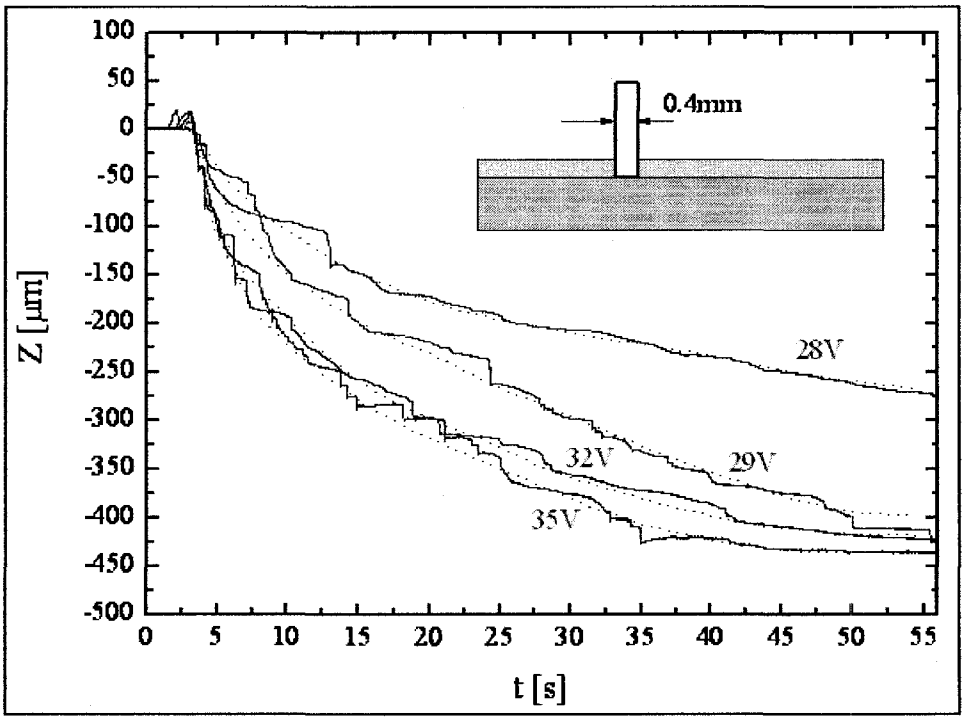

Figure 2: Evolution versus time plot of four samples of micro-holes performed by gravity feed micro drilling at different machining voltages [3].

2.1.3 Gravity feed micro-drilling sequences and procedure

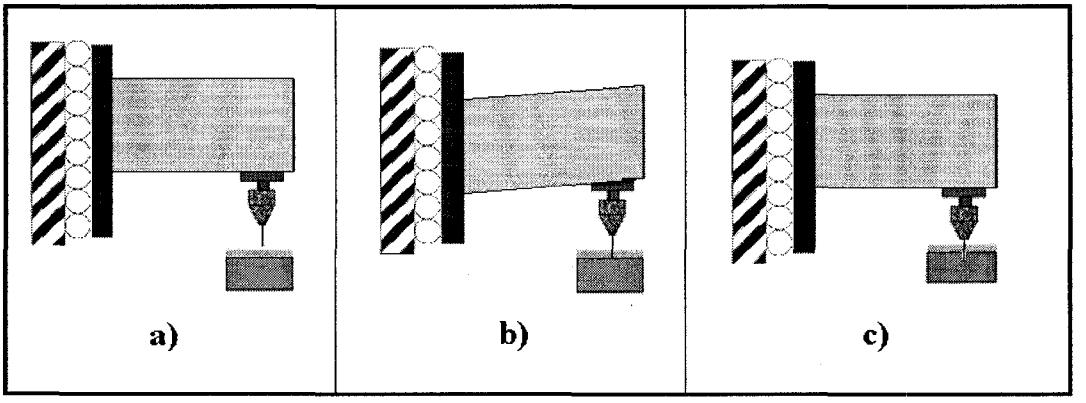

Figure 3: Sketch of the SACE gravity-feed micro-drilling procedure.

Gravity Feed Micro-Drilling (GFMD) drilling was first presented by Kurafuji and Suda [2]. The procedure that is the object of the present study is the one introduced by Wüthrich et al. [7]. The work-piece is initially placed and clamped in position. The electrolyte is then poured inside the electrolyte container, in which the work-piece is immersed. After the initial preparation, the micro-drilling starts by detecting the surface of the work-piece. Subsequently, the power is switched on at a constant voltage. The flexible holder leaves the tool electrode to move freely downwards, penetrating the work-piece due to the electrochemical discharge activity (figure 3).

Figure 4 shows the machining set-up used for research purposes. The optical sensor detects the motion of the tool electrode during the drilling. Calibration of the optical sensor with the displacement of the tool is performed.

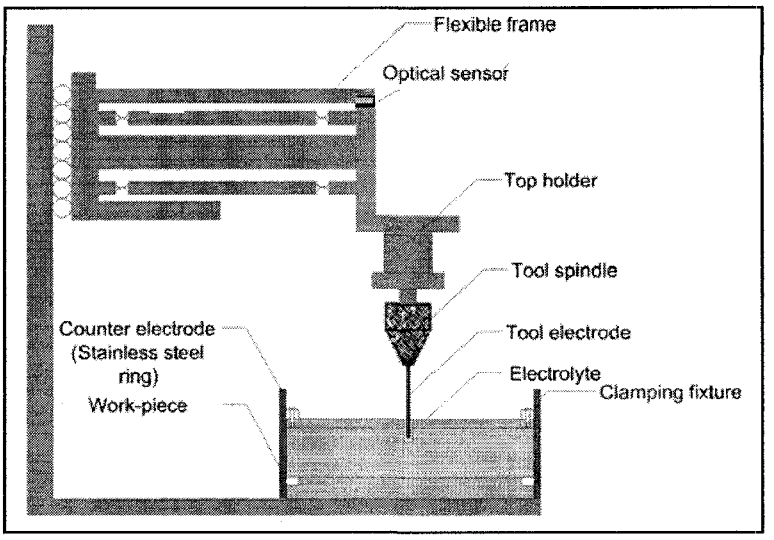

Figure 4: Schematic for the initial setup of SACE gravity-feed drilling [4]. The constant force refers to the weight of the drilling head (flexible frame, Top holder and tool spindle with the electrode.

2.1.4 Drilling regimes

SACE gravity-feed micro-drilling has two different regimes in function of the drilling depth: the discharge regime (depths up to 200-300 μm) and the hydrodynamic regime (depths more than 300 μm) [3]. The discharge regime is controlled by the number of discharges taking place in the gas film (by the applied voltage) [3, 4]. Fast drilling (up to about 100 μm/s) occurs in this regime. On the other hand, the drilling speed in the hydrodynamic regime is slower (a few μm/s), because of the shortage of electrolyte inside the micro-hole during the drilling, limited material removal by chemical etching and the drag force exerted on the tool while penetrating in the molten work-piece [3].

The hydrodynamic regime is strongly non-desirable. On one side it increases the drilling time, and on the other side it is responsible for lowering the micro-hole quality as structural damages (micro-cracks) of the drilled micro-holes happen in this regime. Solutions were proposed to minimize or to eliminate the effect of the hydrodynamic regime. For constant velocity feed, Gautam et al. [5] were able to demonstrate that adding orbital motion to the vertical motion improves the material removal

rate. Vibration motion of the tool electrode was proposed by Wüthrich et al. [6] and it was demonstrated to be efficient in gravity-feed micro-drilling.

2.1.5 Viscosity of the machining zone within the hydrodynamic regime

Recently a model was presented by Maillard et al. [7, 8] predicting the limiting velocity of hydrodynamic regime in SACE gravity-feed Micro-drilling. Maillard's model is based on the relation between the limiting speed of the tool electrode and the resisting drag force. The drag force is function of the viscosity of the melted zone in front of the tool-electrode. The thermal conductivity of tool electrode controls the amount of thermal energy of the electrochemical discharge removed through the tool. This later leads to temperature variations of the molten work-piece in front of the tool yielding to changes in viscosities.

The dynamic viscosity of the machining zone in front of the tool tip during the hydrodynamic regime is obtained for all the tool electrodes using Maillard's model [7, 8]. This model assumes that the drag force - according to Stokes' law - is proportional to the limiting velocity with a proportionality constant that depends on the radius and shape of the electrode and the viscosity of the molten mixture. As the tool electrode moves through the fluid at the melted zone with a small velocity (i.e. low Reynolds number, $Re < 1$), then Stokes' law can be used as described below:

$$\mathbf{F = 6\pi r\mu V} \qquad (1)$$

where

F: is the drag force exerted on the electrode's tip by the fluid of the melted zone [N]

r: is the radius of the spherical object [m]

μ: is the molten mixture viscosity [kg/(m.s)]

V: is the electrode's velocity [m/s]

2.1.6 Material removal mechanism

Several processes are presumed to contribute in the material removal mechanism [14]. These are generally:

- Melting and vaporization due to electrochemical discharges
- High temperature chemical etching
- Differential expansion of constituents and weathering
- Mechanical shock due to expanding gases and electrolyte movement

In this investigation, only thermal effects and chemical etching were investigated in SACE machining literature.

2.1.7 Chemical etching contribution

An electrolyte composition of NaOH with a concentration of about $30\%\ in\ weight$ is a good choice and is commonly used [2]. If very thin substrates have to be machined, the concentration should be reduced [13]. The mean temperature of the electrolyte affects material removal rate. To the author's knowledge electrolyte level and electrolyte circulation were not yet systematically investigated in SACE machining literature. On the other hand, some studies focused on the promotion of the chemical etching by changing the tool-electrode shape [3], by tool-electrode vibration [6] and tool-electrode rotation [15], or by adding abrasive to the electrolyte [16].

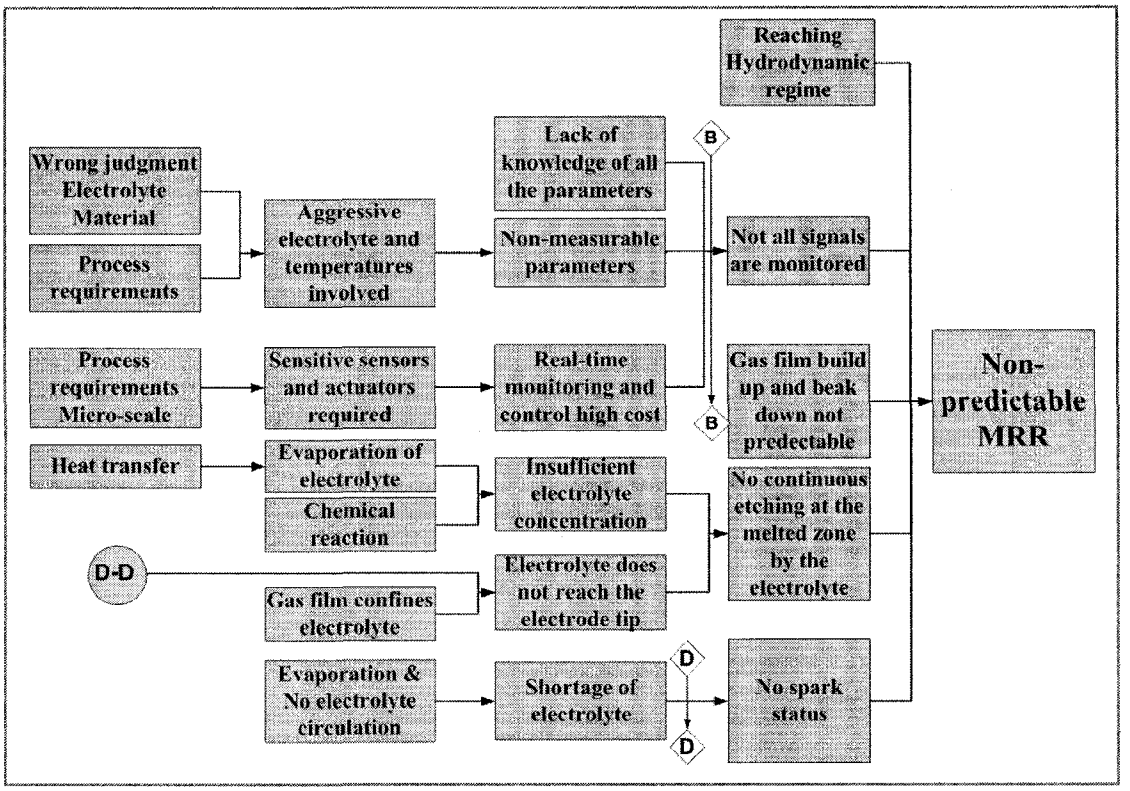

Figure 5: Causes of non-predictable machining removal rate in GFMD.

2.1.8 Heat generation

The heat generated during the machining is a major factor that affects the time of machining (material removal rate) as well as the behaviour and the quality of the micro-holes. For example, reducing the critical voltage [1]by changing the wettability of the electrode electrolyte interface was shown to be efficient [20]. Another efficient way of quality improvement is the utilization of pulse voltage supply. It results generally in excellent quality holes due to the reduction of the heat generated during the machining [10, 11, 12]. Figure 5 shows a cause and effect diagram of non-predictable machining removal rate.

[1] The voltage required for the gas film formation to occur. It is linked with critical current which depends on the current density and the electrode and electrolyte interfacing surface. The current density is 1 A/mm

2.1.9 Repeatability of drilling

GFMD being an open-loop machining process does not stop it from being fairly predictable. However, usually several successively drilled holes are needed before the evolutions become similar. Figure 6 shows typical consecutive evolutions at 29 V in glass with a cylindrical stainless steel tool-cathode of 0.4 mm diameter [3]. It is noted that after about five drilled holes, the evolutions become more and more similar reaching finally a steady state situation. This effect is so far believed to be due to the time needed in order the local temperature and electrolyte concentration to reach their stationary value.

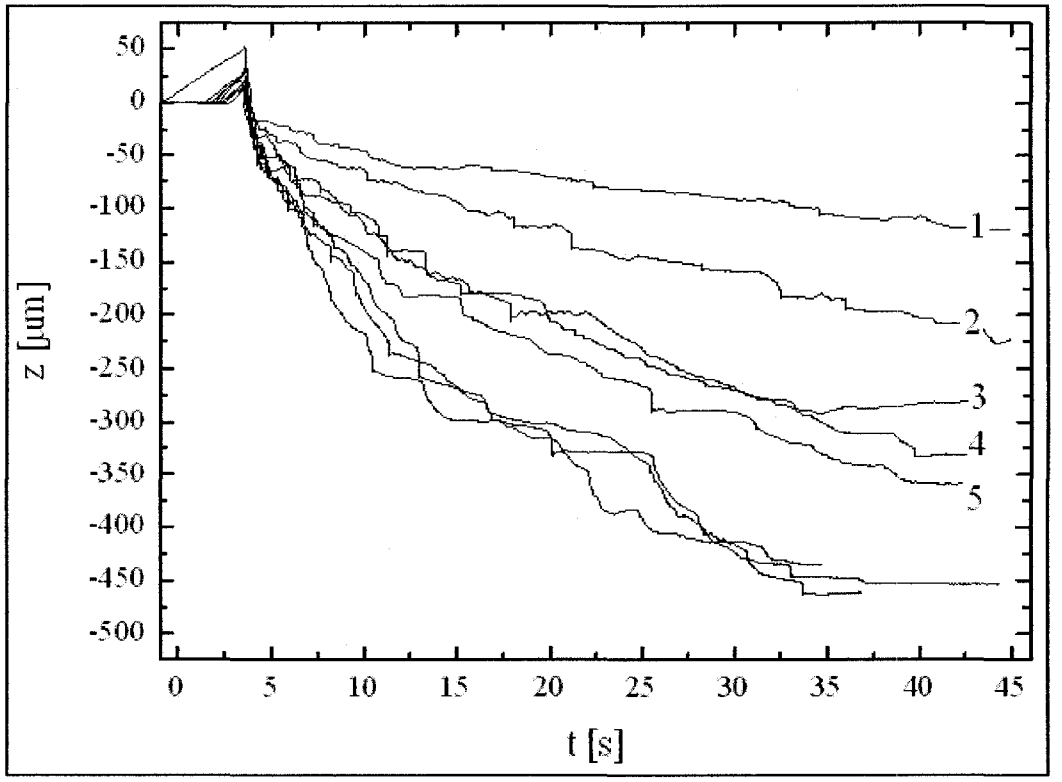

Figure 6: Several consecutive glass gravity-feed drillings at 29V with a cylindrical stainless steel tool-cathode of 0.4mm diameter. Applied force was 0.8N. After five successively drilled holes, the evolutions become similar [3].

2.1.10 Influence of inter-electrode resistance

It is well known that the gas film is unstable (i.e. the gas film often breaks and has to be building up again). The gas film formation time is an important parameter for the mean machining speed of SACE [4] and may become a significant limitation of the drilling speed. The more frequent the gas films build-up and break-up is, the slower the drilling process will be. The gas film formation time is, besides other parameters, controlled by the inter-electrode resistance [4]. Higher resistances results in general a slower gas film formations.

2.1.11 Machining quality

A first quantitative characterization of the micro-hole quality in GFD was presented by Maillard et al. [17]. Five types of micro-drilling profiles were listed. Those profiles are: well-defined circular contours, jagged outline contours, hole with a heat-affected zone, hole with thermal cracks and deformed micro-holes due to tool bending.

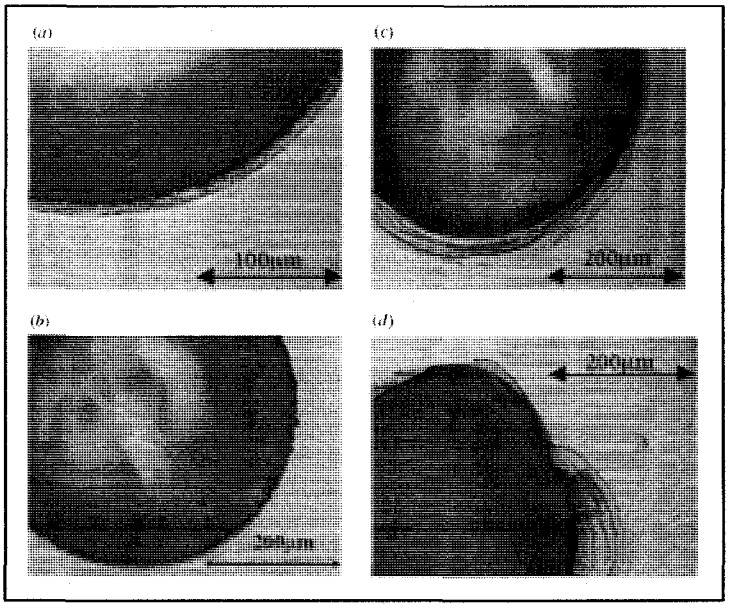

Figure 7: Different micro-hole quality obtained by gravity-feed drilling with a stainless steel 316L tool-electrode of 0.4mm in glass [17].

- **Well defined cylindrical contours with smooth surface (figure 7a):** The entrance of the hole is well defined and characterized by a smooth surface.

- **Jagged outline contours (figure 7b):** The contour is no longer smooth but jagged.

- **Hole with heat affected zone (figure 7c):** The contour remains cylindrical.

- **Hole with thermal cracks (figure 7d):** The hole is characterized by cracks and a large heat affected zone.

- **Deformed holes (figure 8):** The hole tends to be more elliptic in shape. This is caused by the bending of the tool during the machining.

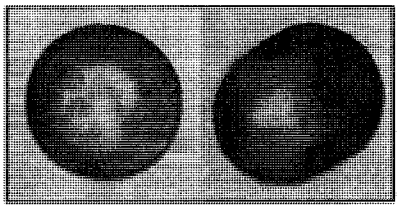

Figure 8: Sample of two micro-holes. Deformed micro-hole because of the tool bending (right) and well-defined circular (left).

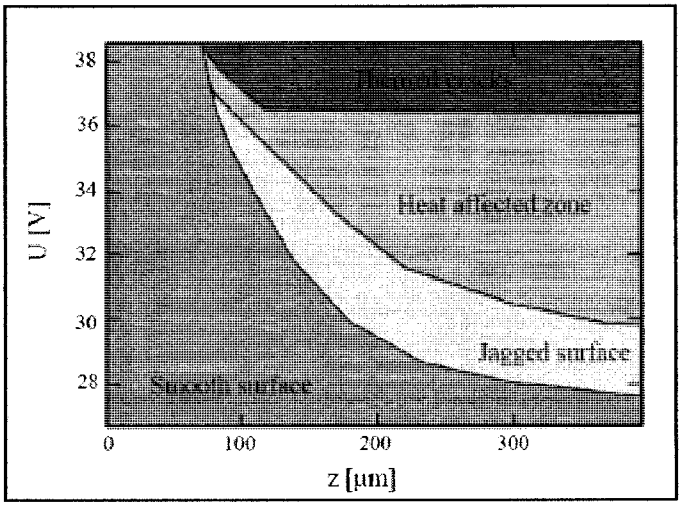

Figure 9: Evolution of SACE glass gravity-feed drilling in the machining voltage U - drilling depth z plane [3].

Figure 9 summarizes the different types of micro-holes that are obtained by gravity-feed drilling in function of the machining voltage and the drilling depth. At the discharge regime (less than 100 μm) higher voltage results in faster drilling without loss of quality. However, as the tool is going deeper into the work-piece, the difficulty in removing the melted material and insufficient wetting of the tool tip increases. This causes the discharge to take place in the upper part of the tool, resulting in a jagged contour and increase of the micro-hole diameter. As the drilling goes on, the micro-hole diameter increases. In this situation the border of the hole is not heated enough to be melted or etched. The micro-hole does no longer increase but a heat affected zone starts growing instead. If the supplied heat power is too high thermal cracks appear.

According this description, deep holes should always have a lower quality than holes with a depth less than typically 100 μm.

Figure 10 shows some factors that cause poor quality in GFMD. The wrong choices of machining voltage, electrode material and geometry or wrong choice of the gravity force seem to be the main causes of the possible poor quality. In edition, the lack of electrolyte and the excess heat contribute in producing micro-holes of poor quality.

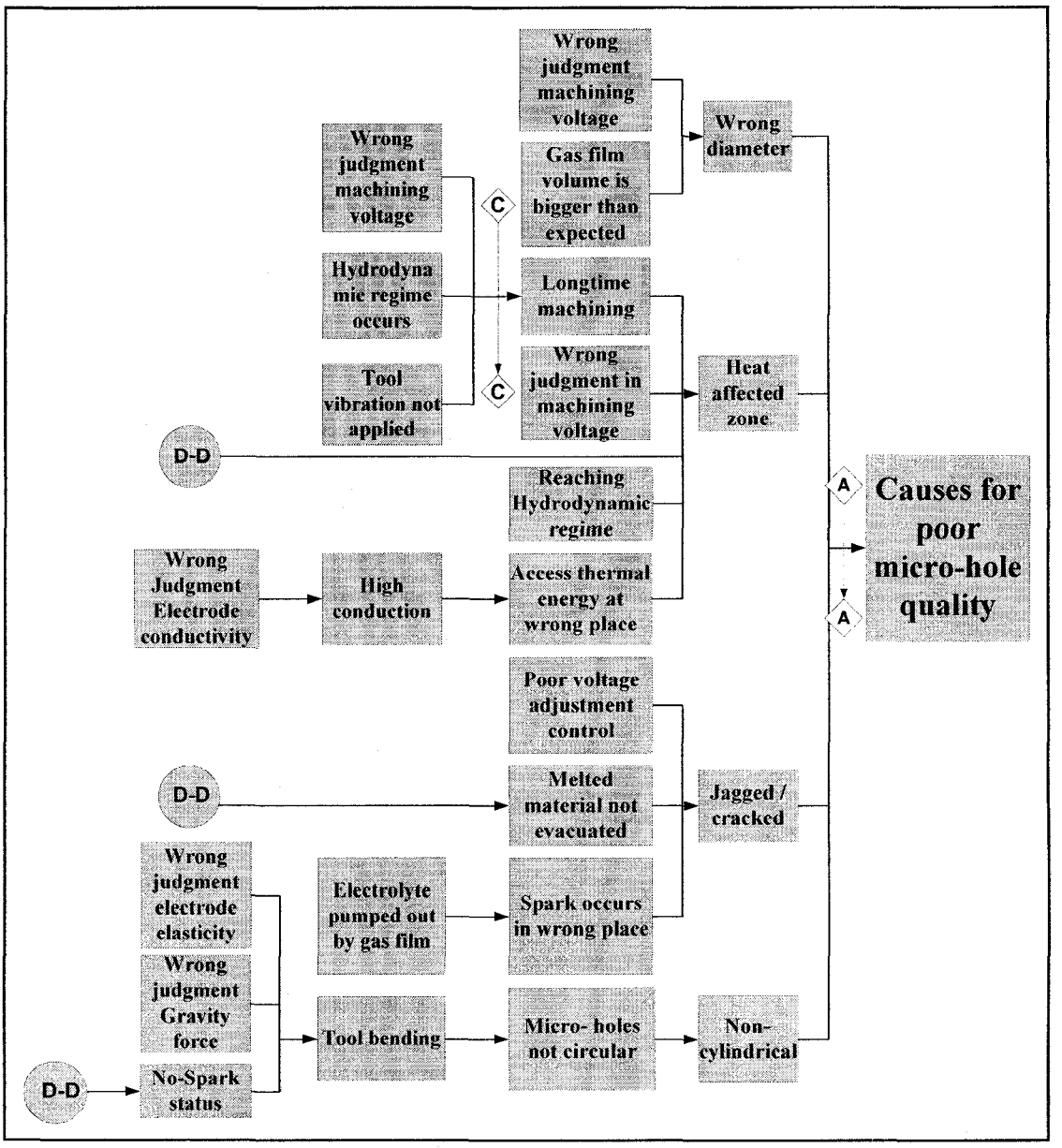

Figure 10: Cause and effect diagram of poor micro-hole quality in GFMD. D-D refers to lack of electrolyte at the tip of tool electrode.

2.2. Quality improvement strategy

According to six sigma techniques (figure 11), there are steps of improvement [18], which are:

- defining the process

- specifying process metrics and measurements

- analysing the measured data and observations

- improving the process.

-control the process by documenting the results and continuously improving the process.

This procedure is suggested to be followed as a guideline for the improvement. Shall this procedure is followed; a new era of improvement can be achieved. This improvement is systematic, unlike the traditional trial and error approaches.

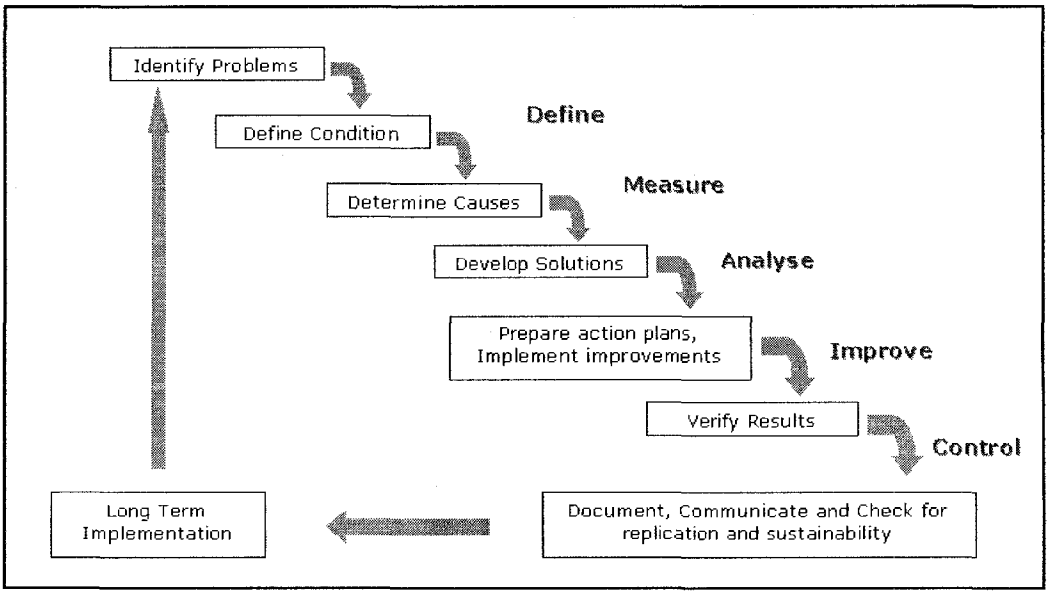

Figure 11: Step by step approach that is followed in this study [18].

2.3. Statistical process control

Statistical Process Control tools (SPC), including cause and effect diagram, pareto diagram, run charts and capability analysis, should be used in order to determine the major causes of the process variability, and then to obtain quantitative indications of the process improvement.

2.3.1 Process definition and initial documentation

The definition of the process is the first step in performing the improvement. Initial documentation such as parameter diagram, cause and effect diagram are required to be created and then continu-

ously updated, in order to ease the handling of the knowledge about the process during the improvement and changes.

2.3.2 Process variability

The variability in a process can be categorized as either common (random) or special caused (assignable) variability [18]. The common cause (chance cause) variability is the natural variability every process experiences. Its existence is due to randomness as we can find purely random variability from one product to another. A process that operates with only common cause variability is said to be *in-control*. The special cause (assignable cause) variability is a result of factors that are not purely random. These factors cause significant differences in the process and as a result they lead to low quality and poor process performance. The process that operates in the presence of special causes of variability is said to be *out-of-control*. This type of variability can be detected with run charts or control charts giving us the ability to remove its effect and therefore reduce the overall variability. As a result, removing special causes leads to an improvement of the quality. In other words guiding the process from *out-of-control* status to *in-control* status shall yield to a better stability in the process. Figure 12 shows a summary of Edward[2] Deming's approach of variability [19].

[2] An American statistician, widely known for his approaches in total quality management and for his recognizable work, on product quality improvement in Japan.

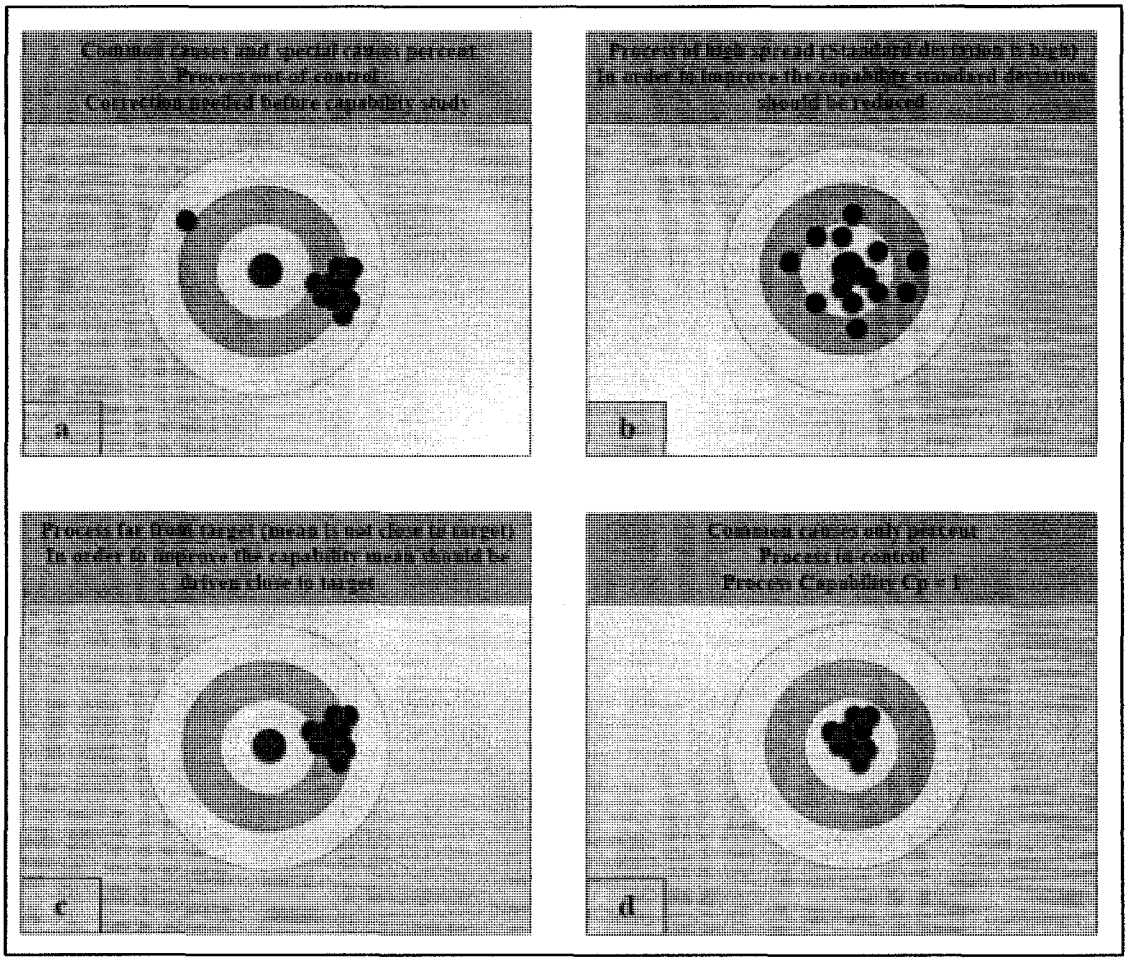

Figure 12: A visual summary of Edward Deming approach of variability [19].

2.3.3 Quality control tools

Cause and effect diagrams, pareto diagrams, process flow charts and run charts are some quality control tools, that are known to assist in determining the major root causes. They are considered as process documentation that should be updated and maintained whenever changes are applied to the process. The changes are considered improvement changes if the process becomes less variable and closer to the target. Figure 5, figure 10 and Appendix A.1 are samples of cause and effect diagrams that is used in this thesis. Appendix A.2 also shows a sample of a pareto diagram similar to those used in this thesis.

Figure 14 outlines the controllable parameters, the noise and fault states. This parameter diagram is followed during the improvement process, and is updated continuously.

Run charts and interval plots are used to assist in the interpretation of data. In run charts the data are plotted onto the charts, the variation of each data is compared around the mean, with the other data, to identify the trend of the process. Similarly the interval plots compare the subgroups accordingly: The rational subgroups are chosen as rows of 10 micro-holes in the drilling set of 50 micro-holes. [18]. Figure 13 shows a dual run chart similar to those used in chapter 4 and 5.

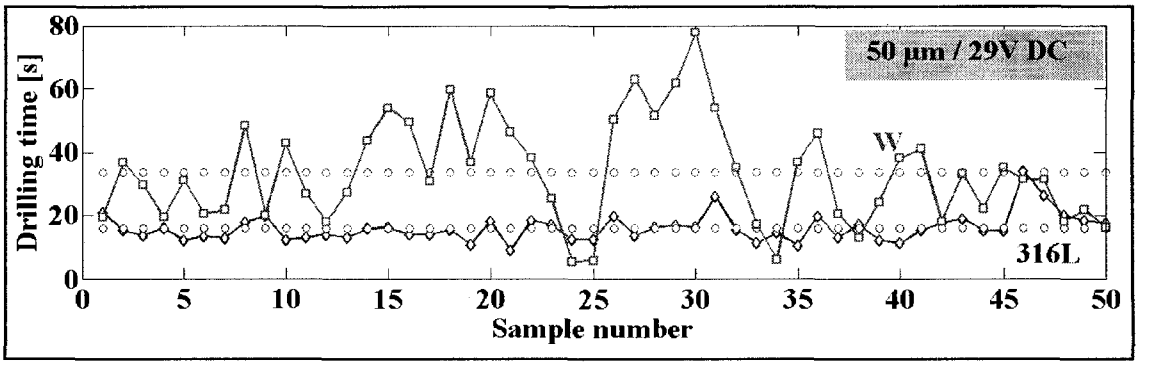

Figure 13: Sample of a run charts. Dual run chart of the machining time with the traditional procedures and with the improved procedures.

Figure 14: GFMD parameters flowchart. This flow chart is built by the author however all the information included is collected from SACE publications.

2.3.4 Process capability

The improvement can be measured in a quantitative fashion using the capability measures, which are:

- Process Capability (Cp) is a simple and straightforward indicator of process capability. And can be calculated as:

$$Cp = (USL - LSL)/6\sigma \qquad (2)$$

Where:

USL: is the upper specification limits

LSL : is the lower specification limits

σ : is the standard deviation of the population

- Process lower half capability (Cpl). Can be calculated as:

$$Cpl = (Mean - LSL)/3\sigma \qquad (3)$$

Where:

Mean: is the mean of the population

- Process upper half capability (Cpu). Can be calculated as:

$$Cpu = (USL - Mean)/3\sigma \qquad (4)$$

- Process Capability Index (Cpk) is an adjustment of (Cp) for the effect of non-centred distribution. And can be calculated as:

$$Cpk = Min(Cpl, Cpu) \qquad (5)$$

The ultimate desired process is the one in which the distribution of the population reside between the upper and lower specification limits. In such process 99.73% of the values measured lie in

interval of width of six sigma (6σ). Calibration and design of experiment are used to drive the process to the desired target and to reduce the variability.

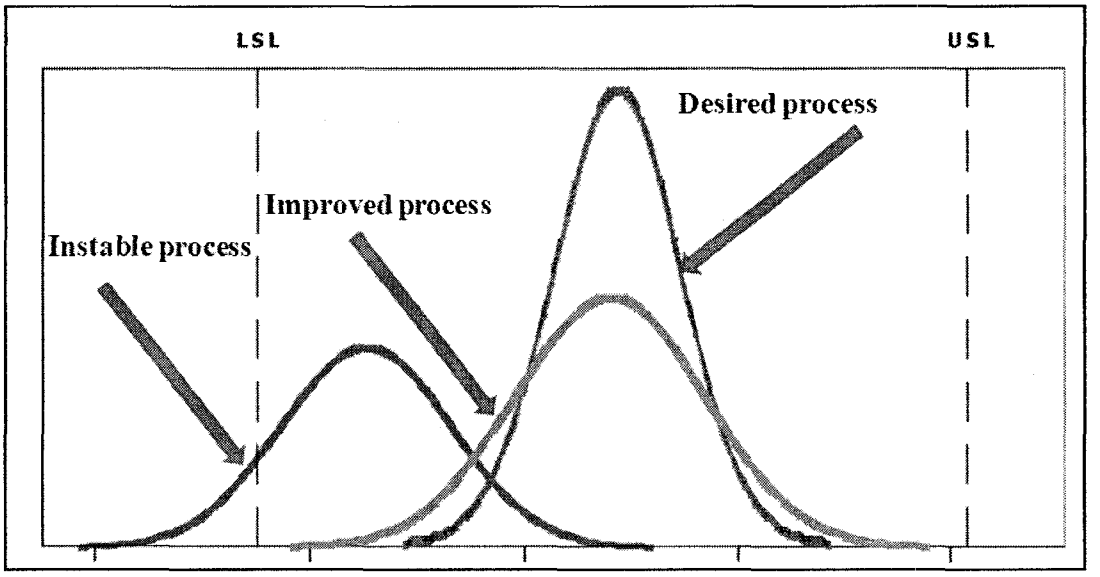

Figure 15: Process capability plots for different stages of the process.

Figure 15 shows thee stages of the process, which are:

- Instable process, where the variability is significant and the process is away from the target.
- Improved process, where the variability is minimized and the process is much closer to the target.
- Desired process, where the variability is eliminated and the process is at the target [18].

2.4. Summary

In this chapter the state of the art of GFMD is reviewed and found to have a potential for improvement. Although it is a cheap and simple process, it has neither predictable machining removal rate nor predictable micro-hole quality. Both thermal and chemical effects need to be focused at. Six sigma policy of improvement is proven to be effective. This improvement will be carried and analyzed in this study and shall be evaluated and measured by using some quality tools such as

capability. Cause and effect diagrams are necessary to determine the major root causes of the non-predictability of both machining removal rate and micro-hole quality. The pareto diagram is then used to determine the major root causes to be eliminated or minimized.

Chapter 3
Gravity feed micro-drilling improvement

3.1. Potential for improvement

In GFMD quality and material removal rate are the most important aspects for improvement. To improve quality, chemical etching should be promoted in order for the machining to progress efficiently. Heat generated in the machining area should be correctly adjusted to avoid heat affected zones and thermal cracks. Other factors relate to the material of the tool electrode and geometry. Furthermore, to improve the material removal rate the following elements are known to be efficient: tool motion (rotation and vibration) and addition of abrasives to the electrolyte. However, the absence of systematic improvement strategies and lack of knowledge about several interactions in the GFMD process are the major breaks towards improvement according to the author's prospective. For example, the absence of improvement strategy yields to disorganized and non-systematic improvement (trial and error approach) which delays the improvement process.

3.2. Thesis outline

Four topics are investigated in this study. Two are industrial engineering concerns and the other two are fundamental aspects about the SACE process. The industrial engineering include presenting an improvement policy and quality investigation. The fundamental study is investigating two major factors in the GFMD which are the heat transfer during the process and the effect of the electrolyte level and temperature on the machining. These aspects, where knowledge is still insufficient so far, are important for further process improvements.

3.2.1 Presenting a strategy for improvement

As discussed in the previous chapter, six sigma procedures are introduced to be a good path to follow during the improvement process. The parameter diagram and cause and effect diagrams are

used to simplify and summarize the considerable amount of knowledge that is accomplished over the years. This builds the first base of process documentation. For the first time something excluding trial and error is introduced. Quantitative measure of the overall process are provided according to metrics that not only linked to quality of the fabricated parts but could be linked to one or more other process metrics like time and non-machining magnitude[3]. Figure 15 outlines the controllable parameters, the noise and fault states. This parameter diagram is followed during the improvement process, and is updated continuously.

3.2.2 Investigating the heat transfer in the process

The interaction between tool-electrode thermal conductivity and both the material removal rate and the quality of the micro-holes are investigated. The effect of the discharge activity and heat capacity coefficient of the tool electrode material shall affect the drilling.

3.2.3 Investigating the pulse voltage

The machining time and micro-hole quality with pulse voltage is studied. They are then compared with those of DC voltage machining.

The results of this investigation showed significant variability that could be related to insufficient control of electrolyte level. This revelled that the electrolyte level is much more significant than considered so far.

3.2.4 Investigating the electrolyte temperature and level

The electrolyte interaction with both the machining removal rate and quality of the micro-holes is investigated. The direct effect of combining preheating the electrode with preheating the electrolyte is noticed to minimize the non-machining magnitude and duration.

[3] Non-machining magnitude is the positive evolution detected by the optical sensor at the first seconds of micro-drilling.

3.2.5 Introducing improvement procedures

Adding the pulse voltage and manual adjustment of the electrolyte to the preheating of the electrode and electrolyte is offered as an alternative procedure. It minimizes the variability and non-repeatability in both the machining time and micro-hole quality.

3.3. Benchmarking

In order to set the goals of improvement, an explicit knowledge about the competitive processes is accumulated. Comparing SACE with other machining processes is completed to know the issues that the improvement should focused at. Although GFMD has some advantages compared to most of those processes - like its simplicity and its cheaper costs-, yet these processes have some major advantages over GFMD especially when it comes to the quality of the machined parts and the production rate. Tables 1 and 2 compare SACE with other micro-machining processes.

Process	$\emptyset_{min}$ [μm]	Aspect Ratio	Removal rate [mm^3/min]	Tolerance [± μm]	Surface finish [μm]	Surface damage depth [μm]
USM	75 [24]	10 [24]	300	7.5	0.2 - 0.5	Low
AJM			0.8	50	0.5 - 1.2	V. Low
LBM	100 [24]	25 [24]	0.1	25	0.4 - 1.25	Med. - High
Milling	500 [24]	10 [24]		50	0.4 - 5.0	Low - Med.
SACE	100 [11]	10 [11]	0.05	10 - 20	0.3 – 1.0 [11]	V. Low - Low

Table 1: A quantitative comparison between ultra sonic machining (USM), abrasive jet machining (AJM), laser beam machining, conventional milling and spark assisted chemical engraving (SACE).

Process	Power Required	Capital investment	Tooling cost	Efficiency	Tool consumption
USM	Low	Low	Low	High	Med.
AJM	Low	V. Low	Low	High	Low
LBM	V. Low	Med.	Low	V. High	V. Low
Milling	Low	Low	Low	V. Low	Low
SACE	Low	Low	Low	High	Low

Table 2: A qualitative comparison between ultra sonic machining (USM), abrasive jet machining (AJM), laser beam machining, conventional milling and spark assisted chemical engraving (SACE).

The use of bechmarking shall be used at further stages of the improvement combined with customer survays and the focus groupes to determine the desired characterestics to be changes. One of this thesis outcomes is to increase the machining removal rate of GFMD to compete with Laser Beam Machining (LBM).

3.4. Summary

This chapter outlined the needs of improvement in the rising technology of SACE. The implemented efforts are listed. The competitive advantage gained by SACE is combining simplicity and low-cost with high aspect ratio and smooth surface finish. As long as these values are well-preserved and intensified, this process will take a share in the market of micro-fabrication.

The major issues that are focused at in this study are the properties of the tool electrode effect on the drilling evolution. Pulse voltage is introduced to minimize the instability of the gas film formation, the preheating of the electrode combined with preheating the electrolyte are introduced to minimize both the non-machining magnitude and duration, and the manual level adjustment is proposed to minimize the variability in the electrolyte level (electrode and electrolyte interfacing surface).

The following chapters shall include the topics related to the thermal properties of the tool, improvement procedures and the quality evaluation of the traditional and new approaches.

Chapter 4
The heat generation in gravity feed micro-drilling

4.1. Introduction

This chapter studies the effect of thermal conductivity of tool electrode material on the evolution of the tool electrode in both the discharge regime and the hydrodynamic regime. The non-machining status, occurring in the first seconds of machining, assessment of its root cause and proposed solutions are introduced and tested. Moreover machining with pulse voltage is implemented and investigated. The importance of electrolyte level especially in pulse voltage machining is discussed.

The need for investigating the heat generation in GFMD comes from the fact that not all the supplied energy is used in the machining. As shown in figure 16 a portion of this energy is lost through the tool electrode, the electrolyte and the surrounding environment, i.e., air. The remaining energy is available for machining of the micro-holes. In order to have a better understanding of the influence of these losses, this investigation is necessary. This is especially important as many parameters are yet unknown and almost impossible to predict in a reliable fashion. This makes the simulation of the process very complicated or rather impossible. Therefore, the experimental investigation appears to be the best choice.

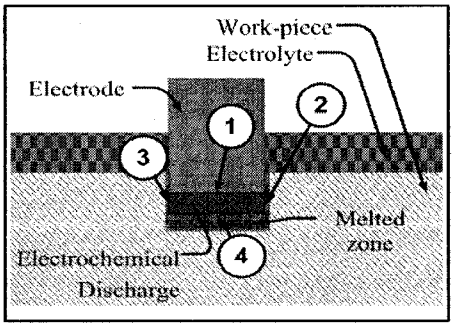

Figure 16: Sketch of the heat transfer in gravity feed micro-machining. The heat is transferred by conduction to the tool electrode (1), by conduction and convection through the electrolyte (2 and 3) and by conduction and convection through the melted zone (4).

4.2. Thermal conductivity of tool electrode

This investigation is performed in order to evaluate the effect of thermal conductivity of the tool electrode material in both the discharge regime and the hydrodynamic regimes.

4.2.1 Experimental procedure

The experimental setup for theses series of experiments is similar to that described in figures 3 and 4. A controlled output power supply provides the required machining voltage (constant voltage) between the tool electrode and the counter electrode. In addition, an optical sensor measures the tool evolution in real time.

The work-piece is initially placed and clamped in position. The electrolyte is then poured inside the electrolyte container in which the work-piece is immersed. After the initial preparation, the micro-drilling starts by detecting the surface of the work-piece. Subsequently the power is switched on at a constant voltage. The flexible holder leaves the tool electrode to move freely downwards, penetrating the work-piece due to the electrochemical discharge activity (figure 3). The force pushing on the tool electrode is 1.90 N. Data are acquired with a frequency of 3.6 kHz for the desired machining time of 60 s. The above mentioned steps are repeated 50 times in order to finish one set of 50 micro-holes. The sketch in figure 17 shows the sequence of drilling for the 50 micro-holes.

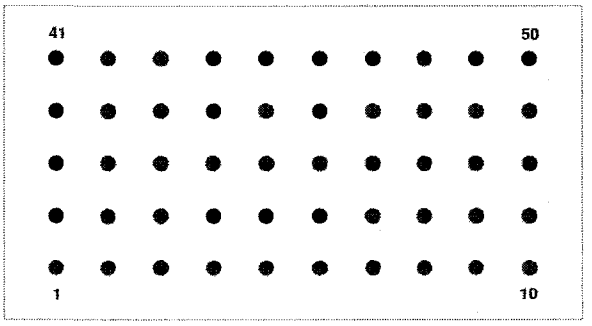

Figure 17: A sketch for a set of 50 holes at the same sequence of drilling used in the experiment.

Data acquisition is performed with an XPS C – 8 controller (Newport) at 3.6 kHz. The power supply is a Lambda Zup 60 – 3.5 operated in controlled output voltage mode. The electrolyte is 30%wt NaOH and the electrolyte level is adjusted between 1 and 2 mm above the work-piece surface. Additional electrolyte is added if needed in order to keep the level constant during the machining. At the beginning of each set of 50 micro-holes the temperature of the electrolyte is room temperature. The counter electrode (anode) is a stainless steel ring of 10 cm in diameter. The tool electrodes (cathode) are cylindrical rods of 0.5 mm in diameter chosen to be from four different materials with various thermal properties: stainless steel 316 L, high carbon steel, tungsten and copper. Table 3 lists the thermal properties of these four materials. The shapes of the electrodes are inspected with an optical microscope and if necessary corrected using emery paper. The work-pieces are Menzel-Gläser 76 × 26 mm microscope slides with a thickness of 1 mm.

Material	Thermal Conductivity W/(m • K) at 300 K	Specific Heat Capacity J/(kg • K) at 300 K	Thermal expansion rate μm/(m • K) at 300 K
Stainless steel (316L)	16	500	15.9
High carbon steel (HCS)	50	472	11.0
Tungsten (W)	173	134	4.5
Copper (Cu)	401	385	16.5

Table 3: Thermal properties of the four tool electrode materials used in this study.

A total of sixteen sets are drilled. Each four of them are machined using one of the four different tool electrodes with a machining voltages of 28, 29, 32 and 35 Volts. The data is analyzed using Matlab. The first 10 micro-hole data are ignored and the average of the data of the rest of the 40 micro-holes is calculated. Neglecting the first 10 micro-hole data is based on the observation that after 10 micro-holes a steady state evolution is reached.

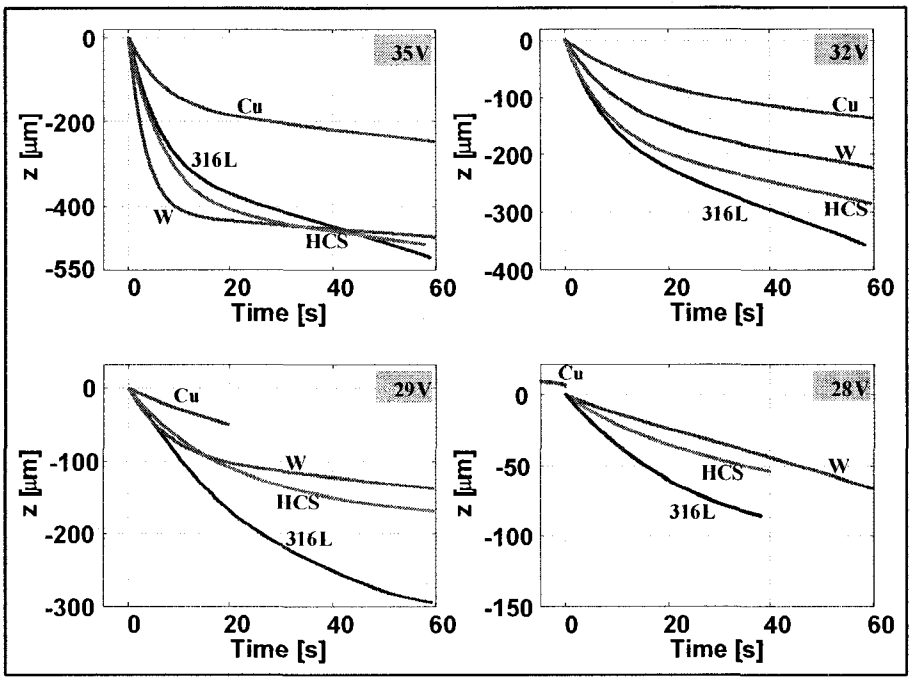

Figure 18: Typical mean evolution of drilling for 0.5 mm diameter stainless steel(316L), high carbon steel (HCS) tungsten (W) and copper (Cu) electrodes, at various machining voltages (28, 29, 32 and 35 V).

4.2.2 Micro-drilling evolution

Figure 18 shows the typical mean evolution of micro-drilling with time for stainless steel 316 L, high carbone steel, and tungsten and copper electrodes at different machining voltages. Let us first discuss the situation for stainless steel 316 L, high carbon steel and copper. It is apparent that the higher the thermal conductivity of the electrode is, the slower the machining is. This is attributed to the increased amount of thermal energy transferred through the electrode to the surrounding media with increased thermal conductivity of the electrode. Consequently, less thermal energy is available for the micro-drilling. The temperature in the machining zone will therefore be lower, resulting in higher viscosity of the material in the machining zone compared to the drilling with electrodes of low thermal conductivity. This yields to slower evolution because gravity-feed micro-drilling is limited by the drag force exerted on the tool in the hydrodynamic regime.

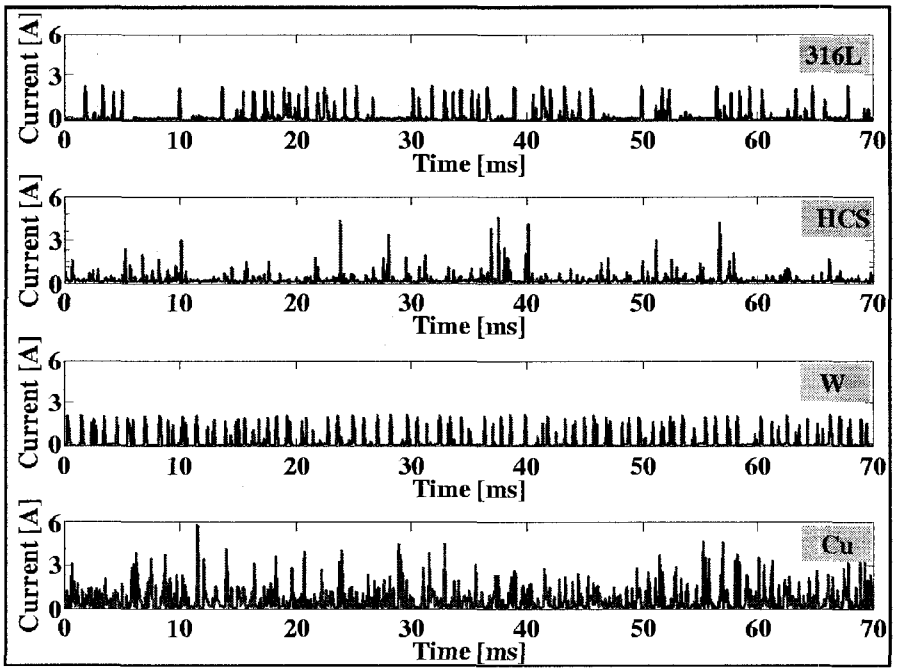

Figure 19: Current signals versus time of the electrochemical discharges for stainless steel electrode (316L), high carbon steel (HCS), tungsten (W) and copper (Cu) at 35V.

Note as well the case of copper electrode. The thermal conductivity is the highest of the three materials. At low voltage, drilling can almost not be achieved. Too much thermal energy is removed through the tool from the machining zone in order for the material removal to take place. Cooper has a so high thermal conductivity, that it transfers very quickly the heat to the machining head. Consequently the copper tool-electrode will have only low temperature increase. This will not favour the formation of the gas film. As can be seen on figure 19, showing the current signal at 35 V, in the case of the copper electrode not only discharges (peeks shorter than the millisecond) but as well several gas film formations (peeks of a few milliseconds duration) are present. This is an indication of the instability of the gas film. The presences of these successive gas film reformations are responsible of the slow material removal rate [4].

Tungsten electrodes behave differently. Even the thermal conductivity is higher than stainless steel and high carbon steel, the drilling is faster at high voltage. This is particularly striking in the discharge regime where the drilling speed is controlled by the number of discharges. The reason for

this is that the number of discharges for tungsten is higher than the number of discharges of the other materials studied as illustrated on figure 19. This can be explained if one recalls that electro-chemical discharges are most likely due to field assisted thermo emission [9]. Tungsten is the only material in the series considered with high thermal conductivity and low heat capacity. Consequently a significantly higher temperature increase of the electrode will result than for the other materials. As tungsten presents a higher discharge activity, the discharge regime will be most affected. This is well seen on figure 20 showing the initial drilling speeds for the four electrodes in function of the machining voltages. Note how tungsten becomes faster and faster with increased voltage compared to the other materials.

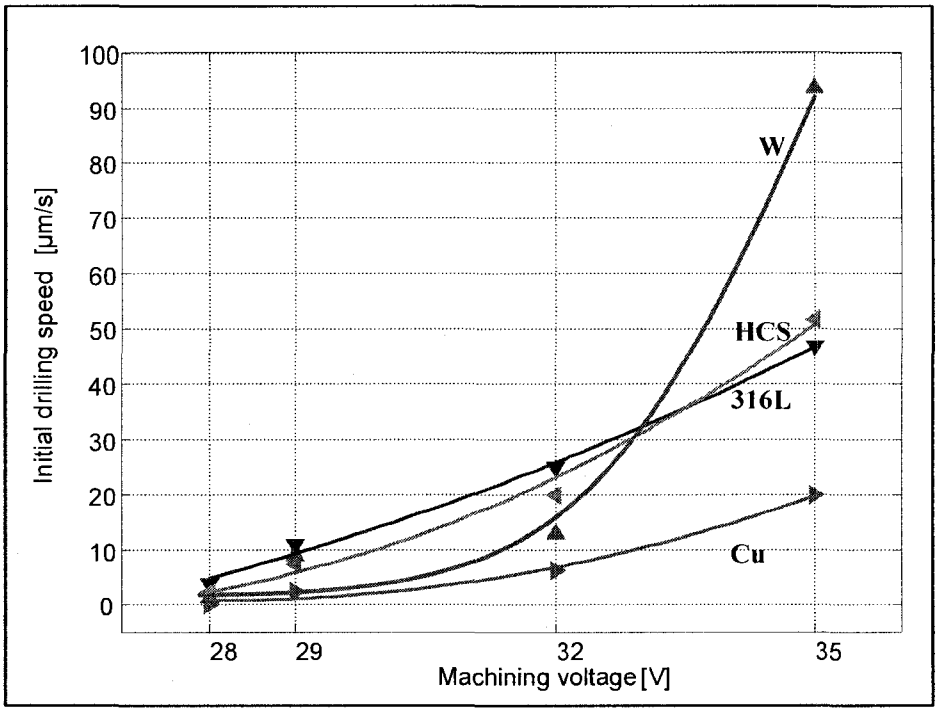

Figure 20: The initial drilling speeds according to the slopes of the fitted curves at the start of the drilling, for 0.5 mm diameter stainless steel (316L), high carbon steel (HCS), tungsten (W) and copper (Cu) electrodes, at various machining voltages.

4.2.3 Viscosity of the machining zone within the hydrodynamic regime

The dynamic viscosity of the machining zone in front of the tool tip during the hydrodynamic regime is obtained for stainless steel and tungsten electrodes using Maillard's model [7, 8]. Knowing the force used in gravity-feed micro-drilling (1.9 N in the present experiments), an estimation of the viscosity in the machining zone can be given. The values of viscosities obtained are 1.7×10^8 kg/(m • s) for stainless steel 316 L electrodes, 2.9×10^8 kg/(m • s) for high carbon steel, 3.3×10^8 kg/(m • s) for tungsten electrodes and 3.9×10^8 kg/(m • s) for copper electrodes. As expected, the higher the tool electrode thermal conductivity is, the higher is the viscosity in the machining zone.

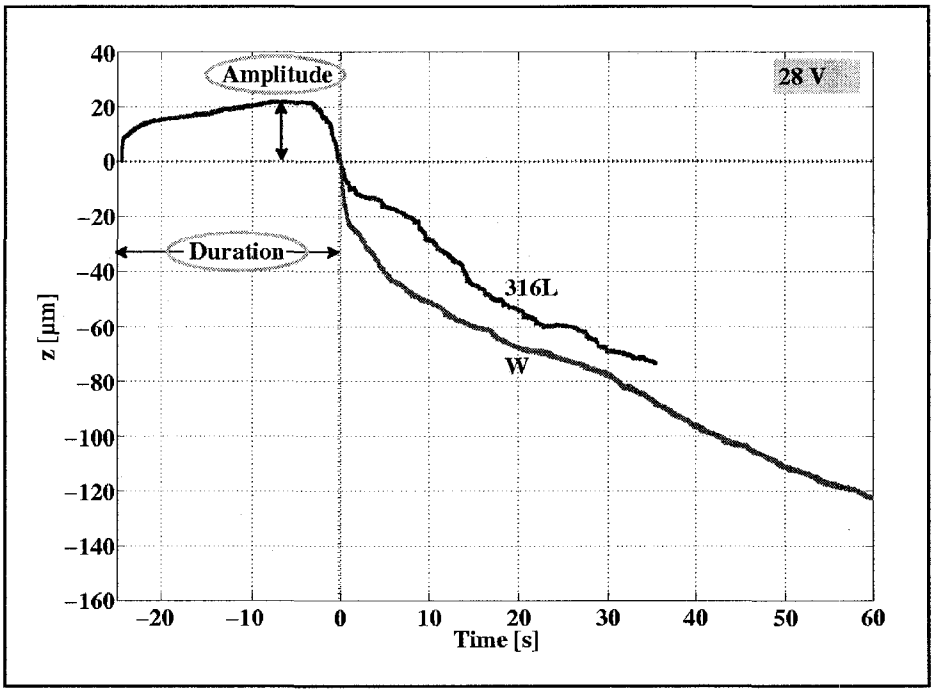

Figure 21: Evolution of drilling depth as a function of time for stainless steel (316L) and tungsten (W) electrodes with a diameter of 0.5 mm, at 28 V machining voltage.

4.2.4 First seconds of micro-drilling

Figure 21 shows the evolution of the stainless steel and tungsten tool electrodes machining at 28 V. At the start of drilling, one can observe a time interval in which the optical sensor reading for the tool electrode evolution is positive. Micro-drilling with copper electrodes at low voltages follows similar behaviour. In the first 60 s of drilling with copper electrode at 28 V the tool electrode evolution is still positive (figure 18). This behaviour is most probably caused by the linear thermal expansion of the tool electrode's tip. Since the thermal expansion coefficient of stainless steel is about four times larger than that for tungsten's, the thermal expansion is more significant for the stainless steel electrodes. The average of the amplitudes is around 20 m, which agrees with the calculated expansion of stainless steel electrode assuming a temperature changes of 500 K during the drilling. This temperature difference is based on the values measured by Raghuram et al. [26, 27] and Yerokhin et al. [25]. Figure 22 shows the correlation between the amplitude and the duration of the tool expansion region for micro-drilling with stainless steel electrodes at 28 V.

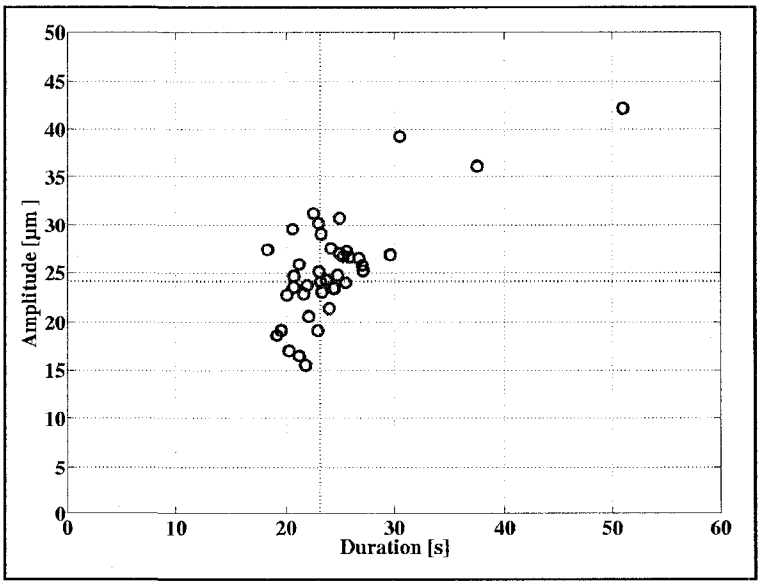

Figure 22: Plot of the amplitudes vs. the duration of first seconds of drilling for the last 40 micro-holes, calculated from the real evolution data for stainless steel 316L electrodes, with a diameter of 0.5 mm, at 28 V machining voltage.

Preheating of the tool electrode before the machining starts is demonstrated to minimize the duration of this phenomenon. Figure 23 shows an example of two micro-holes of different evolution behaviour, one is machined with preheated electrode and the other is machined with an electrode of room temperature at start. The electrolyte is not preheated in both cases and is set approximately to 1 mm level. The tool electrode is stainless steel 316 L. The machining voltage is 29 V (DC). The solution is 30 % wt. NaOH solution.

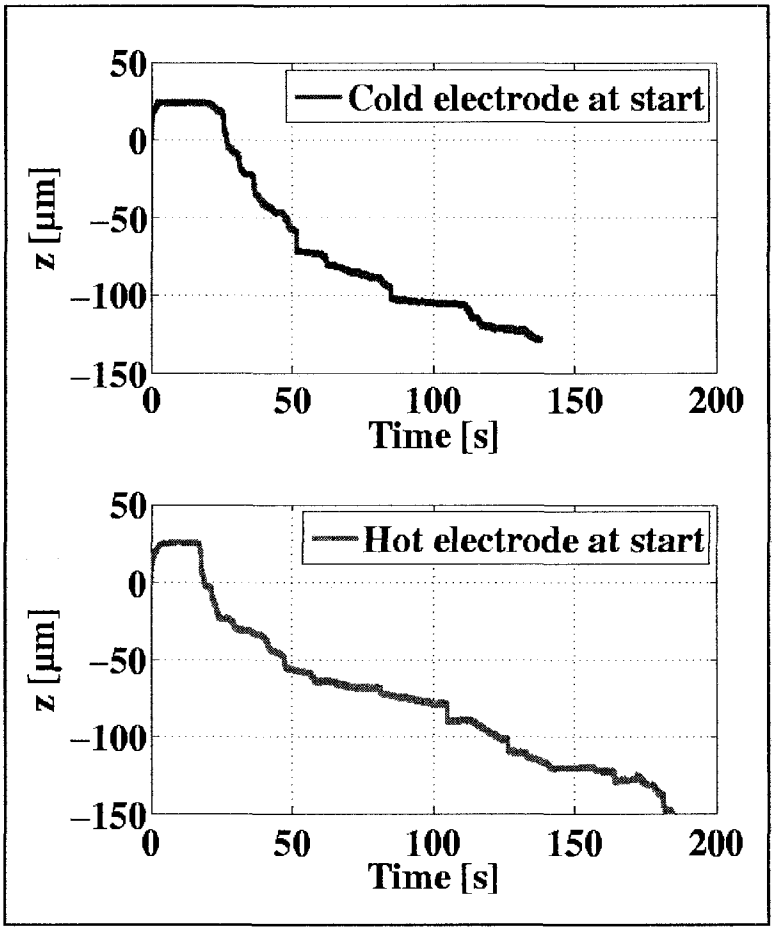

Figure 23: Typical example of evolution versus time plot for two micro-holes: one machined after preheating the electrode and the other one machined with a tool electrode initially at room temperature. Electrolyte level is 1 mm, electrolyte is initially at room temperature.

4.3. Applying pulse voltage

4.3.1 The goal of using pulse voltage

Pulse voltage is implemented experimentally as it was recommended by Zheng et al. [15] for process improvement. Adjusting the ratio between the time-on T_{on} and the time-off T_{off} is useful in two ways. First, the problem of the gas film instability is practically eliminated. So that, by choosing high frequency voltage pulses and small duty ratios $T_{on}/(T_{on} + T_{off})$, the machining can be improved. Second, when the applied voltage is adjusted in timely fashion, the resulting thermal energy at the tip of the electrode is adjusted accordingly.

4.3.2 Pulse voltage Circuit

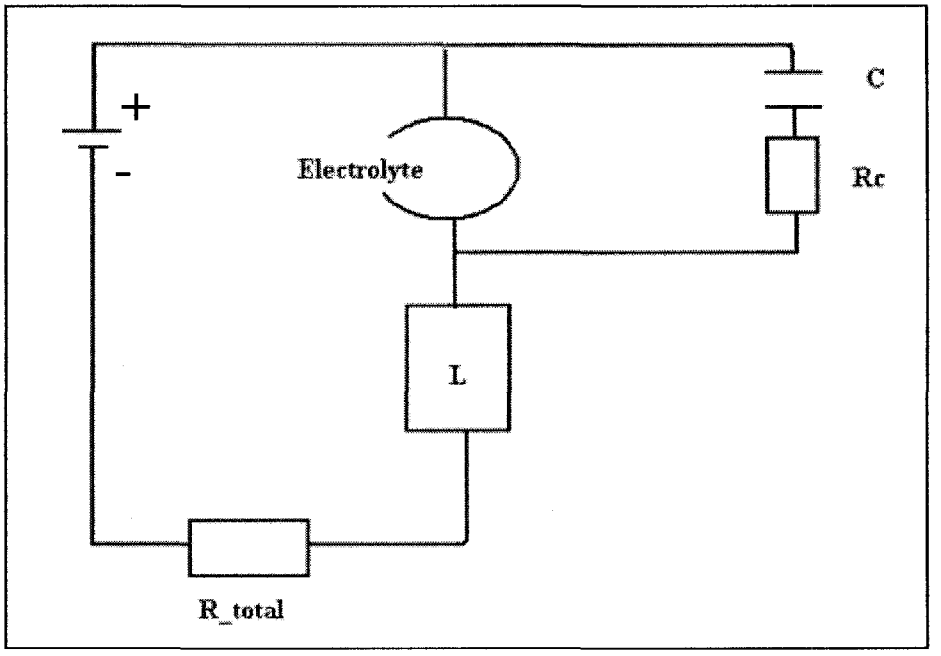

Figure 24: Pulse voltage, time-on time-off circuit, L=8 mH, R=12.8 Ohms, V=29 V electrolyte 30% wt. NaOH.

To produced pulse voltage with the desired values of time on and time off, the circuit shown in figure 24 is used as a result of a prototyping, very similar to Wehnelt's current interrupter[4]. Selection of parameters for the circuit is done taking into account the response time of the power supply and the electrical components. The pulse-on time T_{on} is chosen to be longer than the mean gas film formation time, but short enough to avoid supplying excessive heat to the work-piece [11]. The frequency of interruption can be controlled by inductance of the induction coil, resulting in high frequencies for low values of the inductance [15]. Appendix C.1 discusses the ideal signal to be generated from the proposed pulse voltage. Figure 25 shows the current versus time plot for micro-drilling with pulse voltage in different stages of drilling. It is the first time in history of SACE that this type of circuit is used for pulsed voltage machining. This circuit was chosen for two reasons:

1- To investigate the possibility to use this simple circuit for SACE

2- To investigate the sensitivity of this circuit to the various parameters in SACE

It is demonstrated that such simple circuit is capable of producing a pulse voltage signal which controls both the gas film stability and the heat generation. However it is noticed that the pulse voltage is very reliant on the level of the electrolyte in the machining cell.

[4] The first technological application, presented in 1899, for the electrochemical discharge. Using this interrupter 1000-2000 interruptions per second can be achieved.

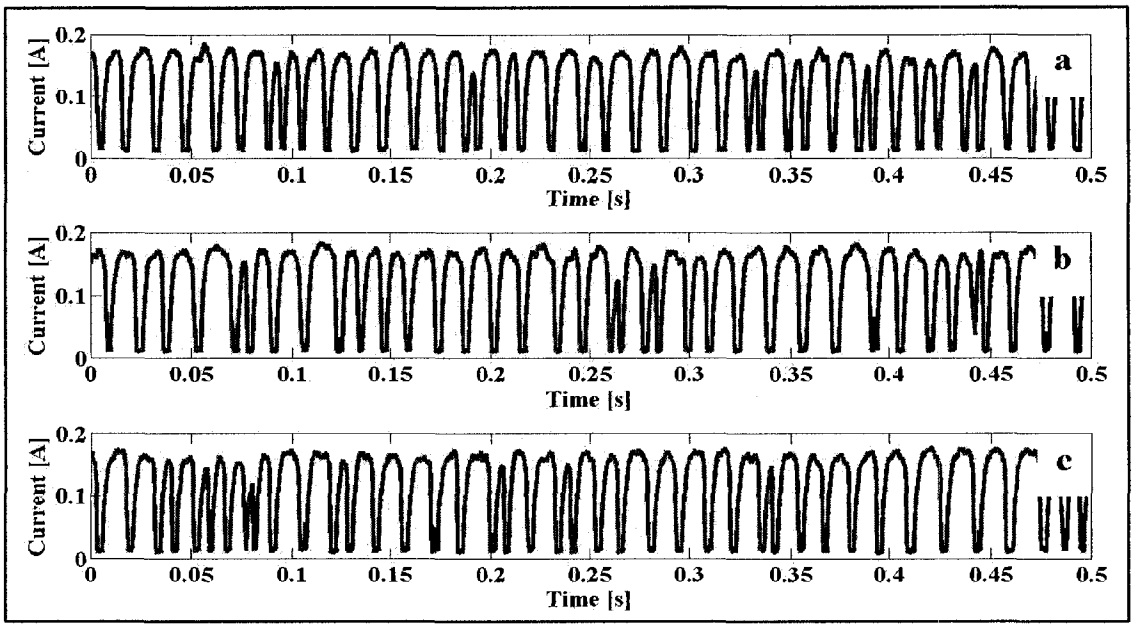

Figure 25: Current versus time plot for micro-drilling with pulse voltage at various depths. a) At the beginning, b) At depth 25μm and c) At 75μm. RLC values are: L=8 mH, R=12.8 Ohms, V=29 V, electrolyte 30% wt. NaOH.

4.3.3 Micro-drilling with pulse voltage

Figure 26 shows a comparison between the first three micro-holes evolution during drilling with pulse voltage or DC voltage. The heat generated during machining with pulse voltage is definitely inferior that in case of machining with DC voltage. This yields to longer non-machining states in case of pulse voltage machining. The evolutions in case of drilling with DC voltage are less variable than those of machining with pulse voltage.

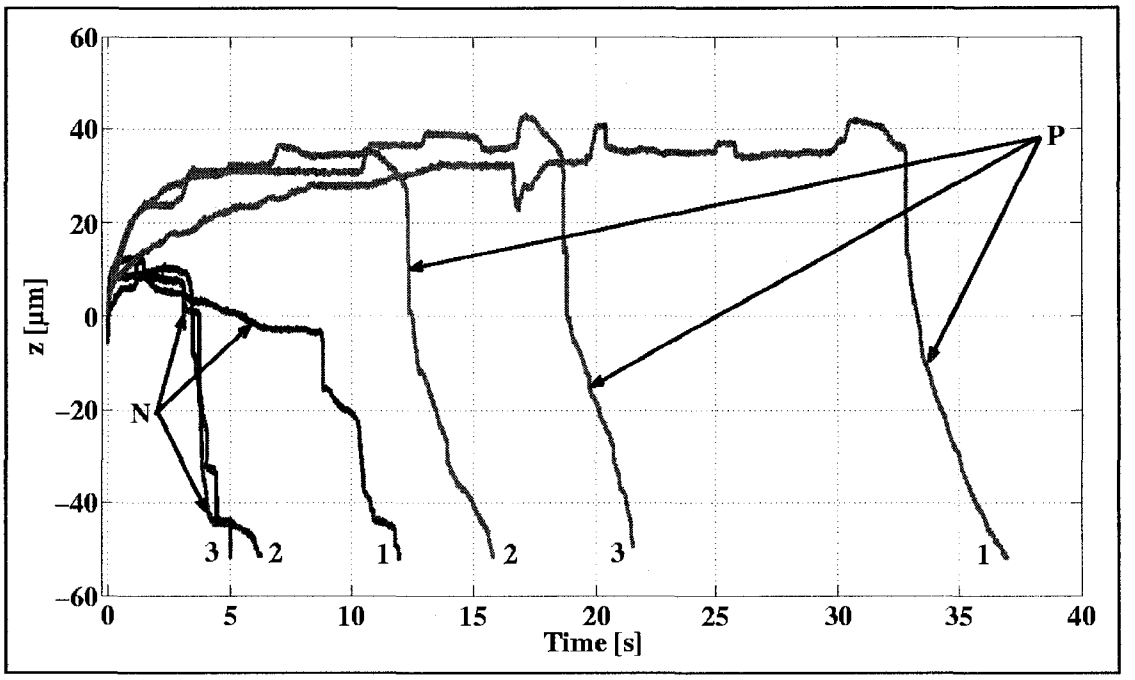

Figure 26: Evolution versus plots of sample micro-drills with pulse voltage (P) and DC voltage (N). The machining voltage is 29 V. The tool electrode is 0.5 mm stainless steel. The electrolyte is pre-heated to 60C and the electrode is preheated.

According to our experiments, it is observed that the issue in drilling with pulse voltage is the level of the electrolyte. High level of electrolyte yields to longer machining. The thermal energy is lost in the electrolyte. To achieve less variability in the evolution of the drilling when machining using pulse voltage, it is recommended to use an adjusted amount of the electrolyte supplied by a programmable syringe pump at the machining area. The amount of the electrolyte needed might be smaller than it could be controlled by a level sensor. Furthermore it is recommended to do more experiments to study the effect of the evolving bubbles that are formed due to the excess of the electrolyte and the white deposits that are formed due to the shortage of electrolyte.

4.4. Electrolyte level and temperature

4.4.1 The importance of electrolyte level

The importance of the electrolyte level became evident during the pulse voltage machining investigations. Although pulse voltage machining is known for the excellent quality of its micro-holes machining, remarkable variability of micro-holes quality is observed in our experimental investigation. The reason is the way we apply the pulses which are highly dependent of the electrolyte level. The variation in level caused a remarkable variation in the time of machining and a remarkable variation in the quality of micro-holes as well. It was therefore decided to do further investigations about the effect of the electrolyte level. Appendix C.2 discusses the theoretical aspects behind the electrolyte level.

4.4.2 Electrolyte circulation and leveling system

On the other hand, it is noticed that the desired electrolyte level with pulse voltage machining is very low. Such low-level could be hard to detect using level sensors. . A proposed solution to adjust the level of the electrolyte without a levelling sensor is to make a new machining cell that contains two containers: an inner container with an overflow opening – levelled with the work-piece surface - and an outer container that collects the access electrolyte. This overflow bath should keep the level of electrolyte adjusted, if as long as the electrolyte is continuously fed. However, more advanced system with dispensing droplets of electrolyte at the position of drilling using syringe pump could be used as well.

The implemented electrolyte circulation system equipped with a controlled hot plate with a temperature probe and a steering system is shown on figure 27. The variability of the concentration between the start and end of the machining process is speculated to be not significant. A syringe pump, or diaphragm set of pumps, can be used for the circulation. The diaphragm pump is used in this study.

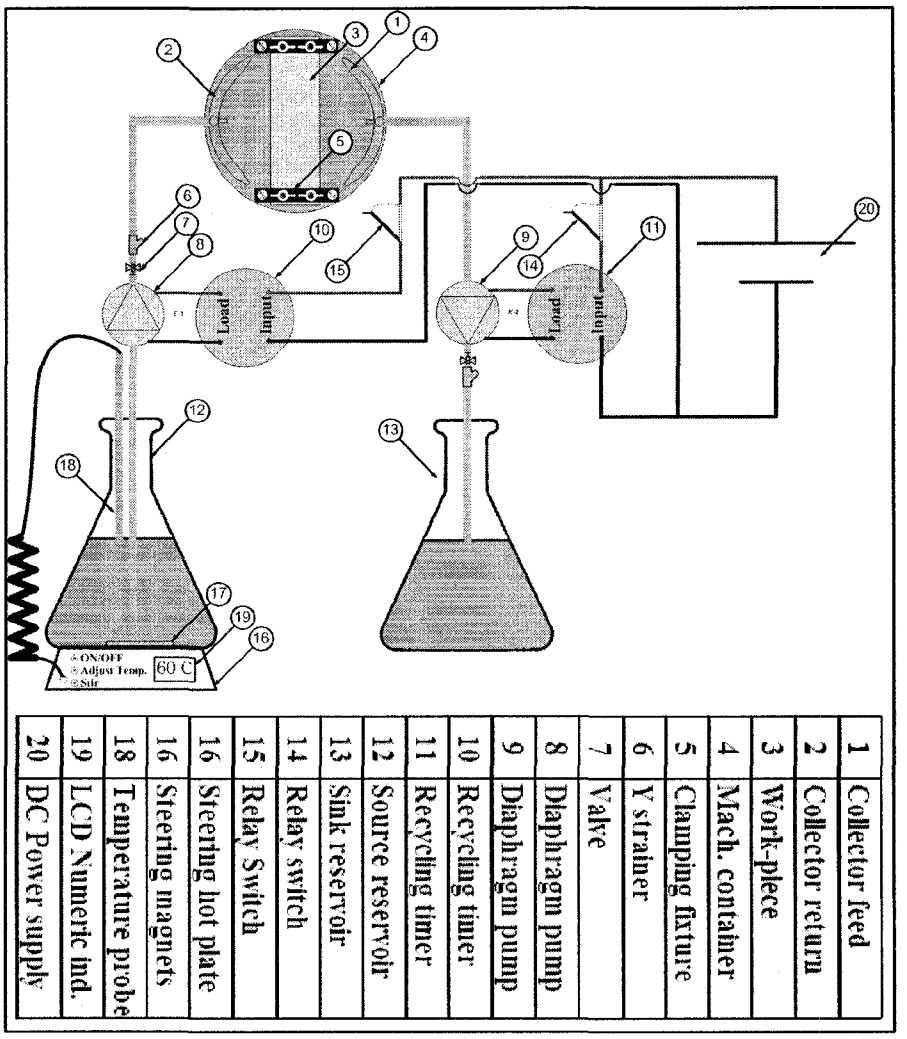

Figure 27: Schematic of the electrical and mechanical components of the electrolyte circulation system. The heating system is a standalone system consisted of hot plate with built in stirrer and temperature probe.

4.4.3 Micro-drilling with different electrolyte level

Figure 28 shows the evolutions plot of six different micro-holes. Three of those are machined with a low electrolyte level (a droplet just enough to wet the work-piece) and the other three are machined with electrolyte of high level (1 mm). The electrolyte is NaOH 30 % wt. solution, initially at room temperature. The electrode is a cylindrical 0.5 mm diameter, stainless steel 316 L. A significant non-machining magnitude - twice the magnitude of non-machining magnitude with high electro-

lyte- is observed. The reason for this might be the gas film which is not developed yet at the start of the machining with low-level electrolyte. Instead some bubbles are formed, pushing the tool electrode upward. The expansion of the tool electrode that causes the non-machining status is not continues any more because of the bubble breakage, this makes the tool go up and down frequently. However it seams that a combination of causes including tool expansion and tool and surface friction force play a major part of this phenomenon.

It is observed as well that low-levels electrolyte yield to faster evolution during the discharge regime and slower evolution during the hydrodynamic regime. In the discharge regime, the small amount of electrolyte in the case of low-level electrolyte is easier to be heated. This heating causes the water content of the electrolyte to evaporate rapidly. As consequence the concentration of NaOH increases locally (under the tip of the electrode), promoting the chemical etching at the melted zone, and causing the drilling to be faster. However when the drilling goes on and reaches the hydrodynamic regime, the electrolyte is consumed rapidly along the way. Until some electrolyte leaks to the micro-hole, a flat region will appear in the evolution curve and reflects the stoppage or slow speed of the drilling.

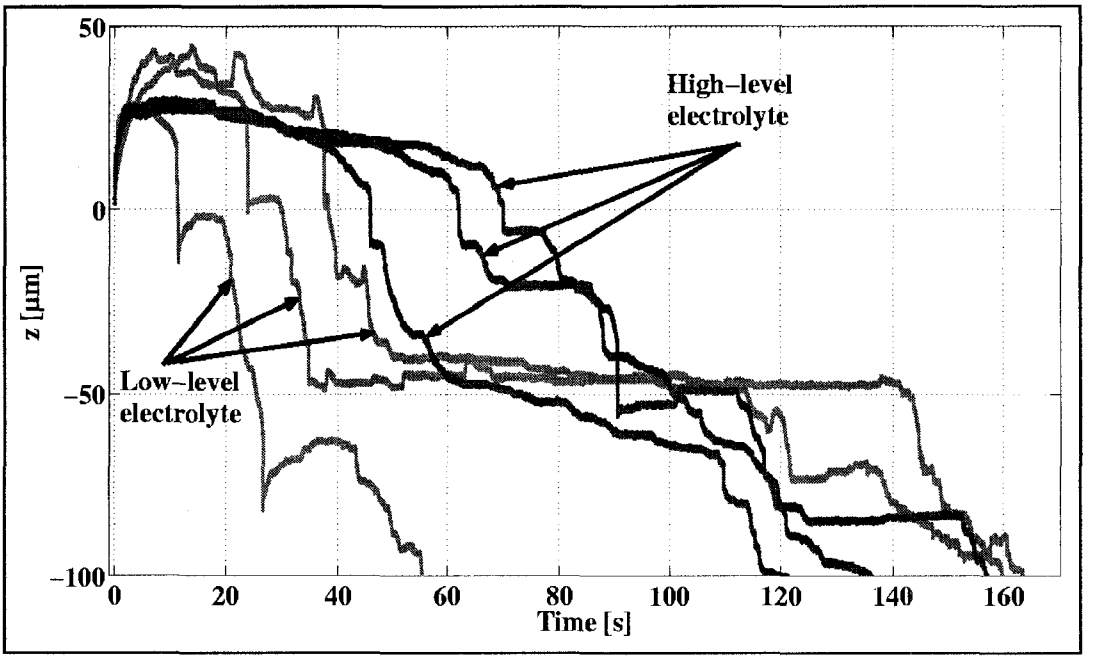

Figure 28: Evolution plots of micro-drilling with high electrolyte level and with low electrolyte level. Machining voltage is 29 V and electrode is stainless steel of 0.5 mm diameter.

4.4.4 Need of preheating the electrolyte

A portion of the supplied input energy is lost in warming up the electrolyte initially (surrounding media of electrode). This energy spreads across the electrolyte volume causing the electrolyte temperature to increase gradually during the machining. According to heat transfer rules, the amount of heat transferred through the media (electrolyte in our case) decreases with decreasing the variation of temperature (between the machining zone and the rest of electrolyte). This is assuming a fairly constant temperature at the machining zone. Preheating of the electrolyte to 60 – 80 °C is suggested and investigated. Yet the choice of initial temperature of the electrolyte might worth some further investigation. Figure 29 shows the evolution plots of two micro-drills. One is drilled with a warm electrolyte (80 °C) and the other one is drilled with cold electrolyte (23 °C). When the hot electrolyte is used, the non-machining duration is reduced to the half. However, in the both cases the electrodes are preheated initially which might explains this significant decline in the non-machining magnitude.

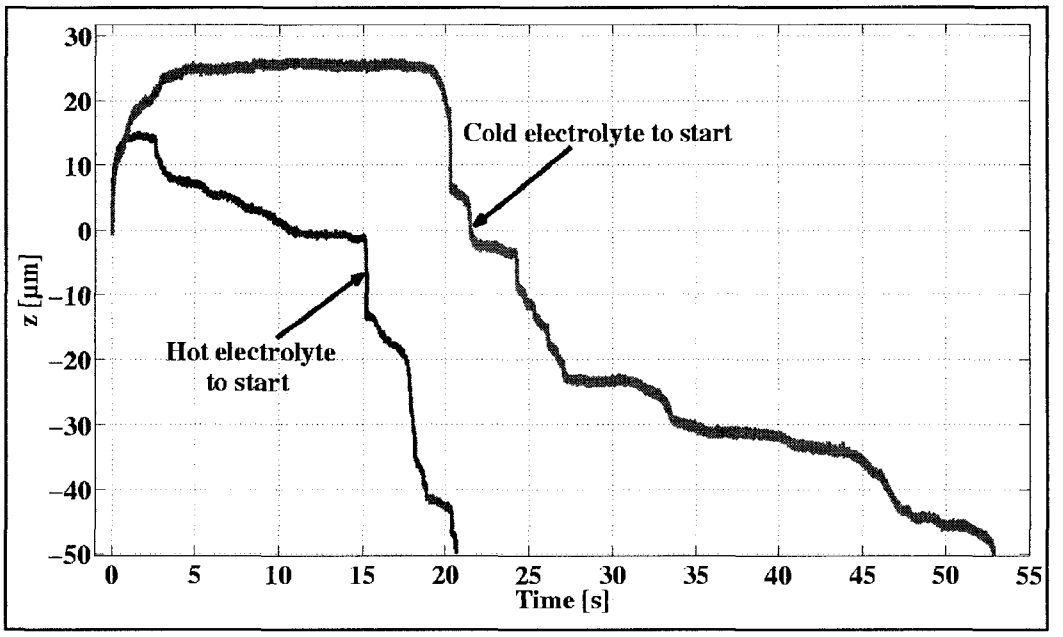

Figure 29: Evolution plots of two micro-drilling one is drilled with 80°C electrolyte and the other one is drilled without preheating the electrolyte initially. Machining voltage is 29 V and electrode is pre-heated before the start of the drilling, and it is 0.5 mm diameter stainless steel. The micro-hole depth is 50µm.

4.4.5 Electrolyte level adjustment and pulse voltage effect on machining time

Figure 30 shows two machining time run charts. In the upper plot the machining is performed after preheating the electrode and electrolyte. And in the lower plot pulse voltage and manual adjustment are combined to the preheating. The variability is reduced. Furthermore the mean machining time is reduced from 99 s in the first case to 59 s in the second case. The gas film instability is minimized and random stair-case like evolution is minimized as well. Instead smooth drilling is achieved (figure 26) with more repeatable machining time.

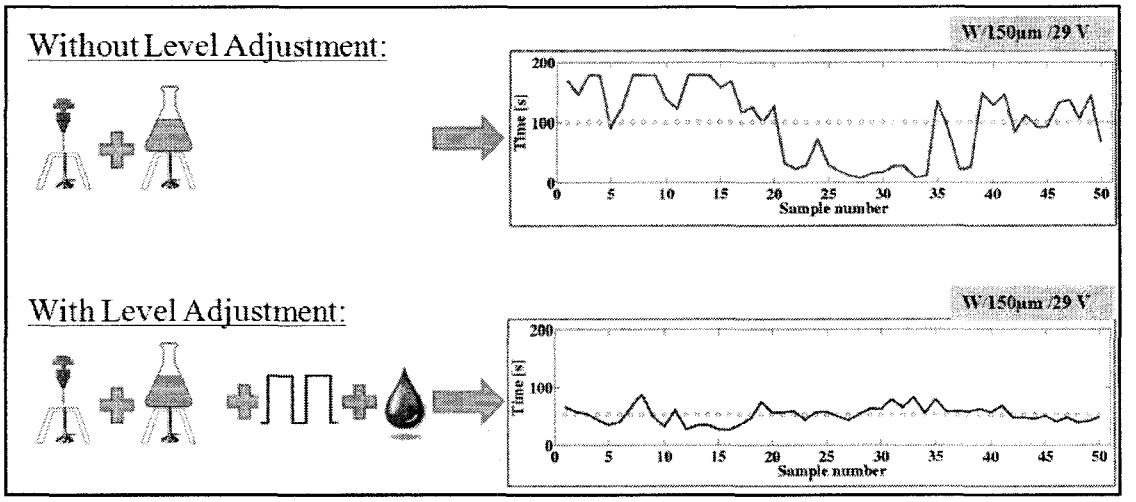

Figure 30: The effect of manual adjustment of the electrolyte level in reducing the machining time.

4.5. Understanding the stair-case-like evolution

Figure 31 shows two categories of drilling. The first category includes a segment in which the drilling slows down or stops forming a stair-case-like evolution, and the second category shows smooth drilling achieved by pulse voltage machining. The flatness region is interpreted as a temporarily slowdown of drilling due to electrolyte shortage inside the micro-hole. This temporary slowdown is ended as soon as electrolyte starts to flow gradually inside the machining zone. The gas film starts to form (possibly combines with bubbles). As a result a positive evolution similar to non-machining status might appears in the evolution plot.

According to this investigation, better interpretation of the process performance is expected to be achieved if the stair-case-like evolution characteristics (magnitude, slope, starting time, etc.) could be measured and studied as metrics. Such metrics might predict the time of machining or the quality of machining or both together.

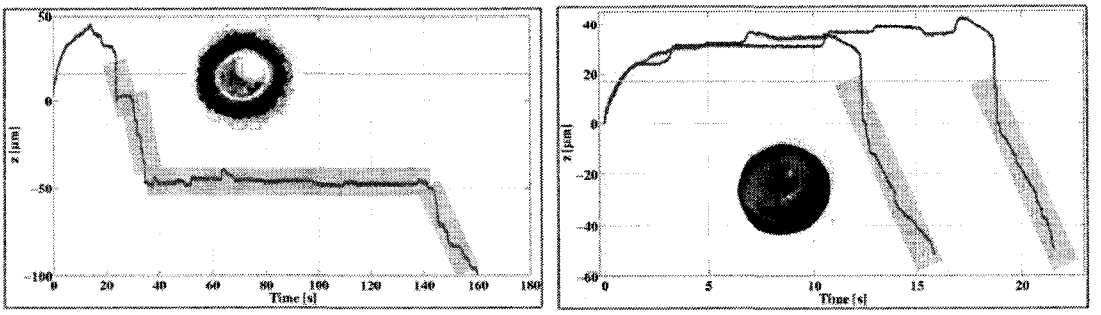

Figure 31: Stair-case-like evolution that indicates slowdown or stopping in machining (right). Smooth drilling achieved by pulse voltage (left).

4.6. Improved process setup

According to the investigation in section 4.3 and 4.4, some improved procedures are suggested, which are:

-Applying pulse voltage which minimizes the gas film instability and produced better repeatability in machining time.

-Preheating the electrolyte and preheating the electrode to minimize the non-machining status.

-Manual adjustment of the electrolyte by adding a droplet of the electrolyte in the top of the work-piece prior to the drilling. This will improve the repeatability of the machining time significantly.

-The machining voltage is 29 V which is chosen, because it is greater than the critical voltage (28 V). It is the best alternative because it yields to smooth micro-hole surfaces with relatively short machining times.

-The electrolyte is NaOH 30%wt. which is proven to yield to smooth micro-hole surface with acceptable machining time.

-The electrode is a circular stainless steel 316L of 0.5 mm diameter. Cut to 1.5 cm in length to minimize tool bending. The cut is done using Electrical Discharge Machining (EDM).

-The traditional machining cell is used and the exerted force is 1.8 N.

4.7. Improving the machining time

A comparison between the traditional and the improved micro-drilling procedures are shown in figure 32. The preheating of electrode and preheating of electrolyte, pulse voltage and manual adjustment of the electrolyte level, cause the variability in the machining time to be reduced and the drilling time to be reduced as well.

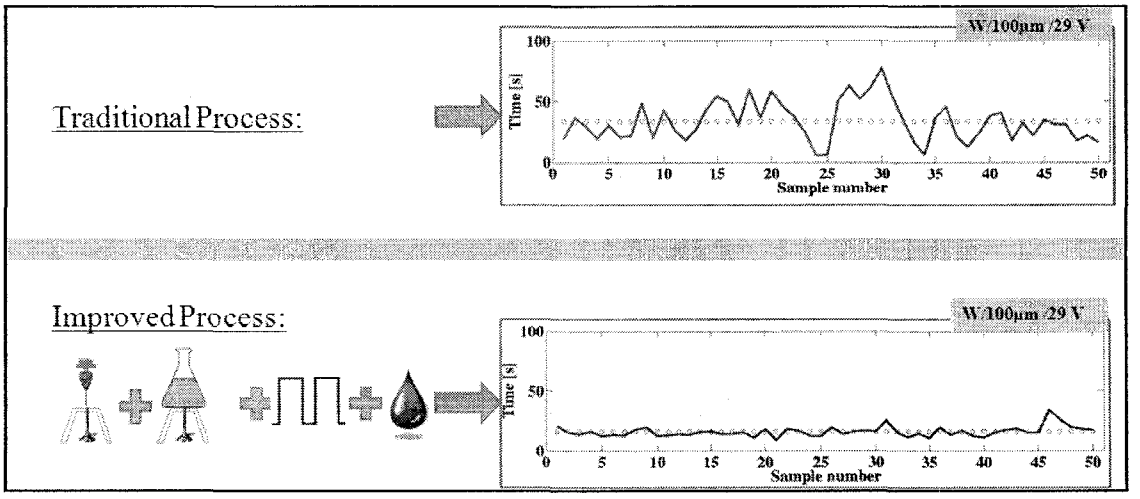

Figure 32: Comparison between the traditional drilling procedure and the improved procedures. The variability in the machining time is reduced and the mean machining time is minimized.

4.8. Summary

The thermal conductivity of the tool electrode controls the heat transfer from the machining zone. The higher the thermal conductivity, the higher is the quantity of heat transferred trough the tool electrode. High thermal conductivity of the tool material results in hotter electrodes during machining and less heat available in the machining zone. The effect on SACE gravity-feed micro-drilling is as follows:

Drilling in the discharge regime is faster for electrodes made of material with high thermal conductivity and low heat capacity as the hot electrode promotes the discharge activity.

Drilling in the hydrodynamic regime is slower for electrodes made of material with high thermal conductivity as the temperature of the machining zone is smaller resulting in higher viscosity of the molten work-piece.

At the first seconds of machining, non-machining status occurs for whatever the type of the tool electrode is. This phenomenon is speculated to be caused by the tool thermal expansion with temperature. To eliminate this effect, preheating of the electrode and preheating of the electrolyte is introduced and tested to minimize the duration of this phenomenon.

When applying the pulse voltage in GFMD. The major factor is the level of the electrolyte. The evolution of drilling in the in case of machining with low level electrolyte is significantly faster in the discharge regime because of the high concentration reached after the evaporation that happens easier in the case of low-level electrolyte. In the hydrodynamic regime, the machining with low electrolyte level tends to slow down significantly because of the lack of the electrolyte in the machining zone.

The tracking and characterization of the stair-case-like evolution may possibly predict the machining process (machining time and/or quality).

Applying the improvement procedures is effective in reducing the variability in the machining time and it causes the mean machining time to decrease.

Chapter 5
Quality evaluation of the process

5.1. Introduction

This chapter studies the quality of micro-holes. An image processing program is customized to evaluate the micro-hole entrance surface characteristics. The process capability is calculated for the first time in this process to evaluate the effect of the implemented improvement.

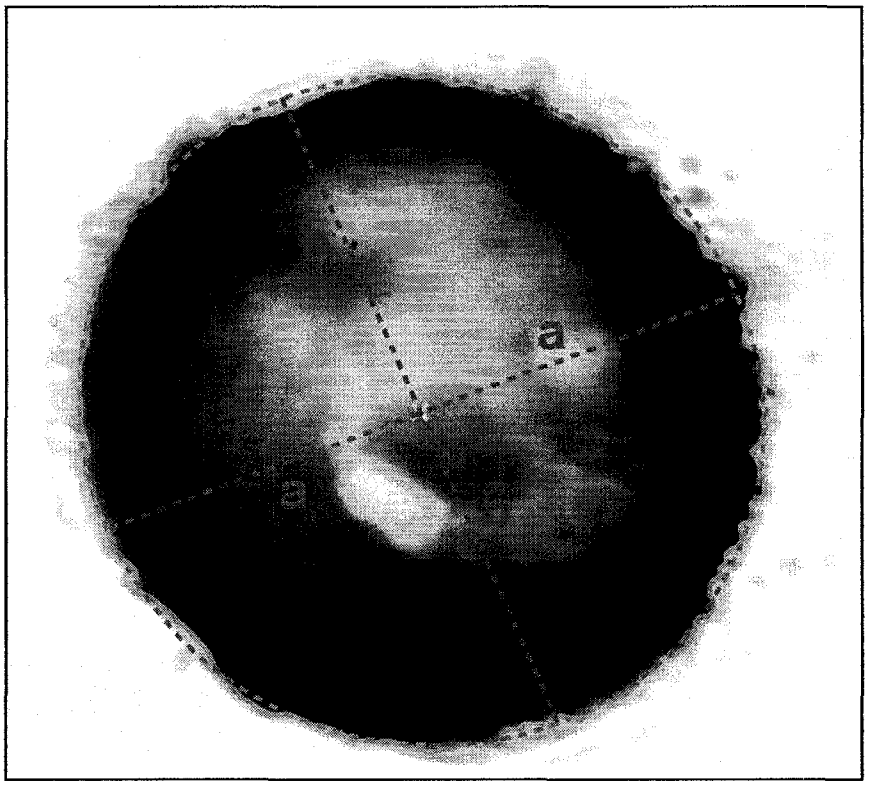

Figure 33: Microscope image of a micro-hole, the vision program tracks the external profile, then ellipse fitting is performed, a is semi-major axis and b is semi-minor axis. (Images are taken by Olympus BX60M microscope with Infinity X digital camera).

5.2. Quality evaluation metrics

An Olympus BX60M microscope with an Infinity X digital camera is used to obtain a photographic image of the micro-holes. An image processing program is customized using Matlab Image Processing Toolbox™ and other special Matlab functions such as (ELLIPSEFIT). A description of the image processing system is briefed in Appendix B.1 Three primary metrics are presented to evaluate the micro-holes quality. Elliptic mean radius, elliptic shape factor, elliptic texture (roughness)

The vision program traces the edges of the micro-hole image. A contour of 1 X 1 pixel unit squares is following upper edge of the micro-hole. Each unit square has an X and Y coordinates assigned to it. This contour is then fitted to the best elliptic shape in order to determine the shape characteristics by Least Squares Ellipse Fit function (ELLIPSEFIT) [23]. Figure 33 shows a sample of a micro-hole image. The major diameter and minor diameter of the micro-hole is measured. Subsequently the mean diameter (or mean radius), the shape factor and the texture are calculated accordingly to the following:

5.2.1 Mean radius

The mean diameter is defined as follows:

$$\mathbf{M} = \mathbf{c}\left(\sqrt{(\mathbf{a})^2 + (\mathbf{b})^2}\right) \tag{6}$$

M: is the mean radius of the fitted ellipse [μm]

a: is the major radius of the fitted ellipse [Pixels]

b: is the minor radius of the fitted ellipse [Pixel]

c: is the conversion factor = $\frac{230}{250}\left[\frac{\mu m}{Pixel}\right]$

The mean radius aggregately compares the quality. The elliptic fitting is not necessary to evaluate the mean radius. Simple circular fitting could also yield to identical results. It is used in comparisons in which the differences in quality of the micro-holes are significant.

5.2.2 Shape factor

The shape factor is defined as follows:

$$\mathbf{SF = b/a} \tag{6}$$

SF: is the shape factor [dimensionless]

The shape factor identifies deformed micro-holes due to tool-electrode bending full figured tool bending (figure 34).

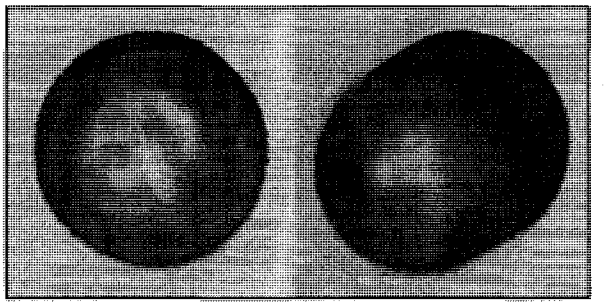

Figure 34: Well-defined circular contour (left) and full figured deformed micro-hole due to tool bending (right) [17].

5.2.3 Texture

The texture of the contour (roughness) of micro-hole image measures the magnitude of convex and concave points on the boundary. The texture is defined as follows:

$$\mathbf{R_{Tex} = \frac{R_p + R_v}{2}} \tag{7}$$

$\mathbf{R_{Tex}}$: is the texture average (roughness) [μm]

$\mathbf{R_p}$: is the absolute magnitude of the maximum convex (peak) [µm]

$\mathbf{R_v}$: is the absolute magnitude of the maximum concave (valley)[µm]

The texture identifies the jagged micro-holes, holes of heat-affected zone and hole with thermal cracks. An error might present when the texture confuses a slight tool bending with that causes a concaves and convex in one direction of the traced contour.

5.3. Quality of the traditional gravity feed drilling process

5.3.1 Traditional machining conditions

This evaluation is originally performed to test the vision system's repeatability. At the same time the machining voltage interaction with quality of the micro-holes is studied. The initial setup with no changes is used for this analysis (the initial setup is described in chapter 4). The voltages chosen are 35V, 32V, 29V and 28V. The tool electrode is a cylinder of 0.5 mm Stainless steel 316 L. A set of 50 holes are drilled during a fixed time interval of 60 seconds . Neither the tool electrode nor the electrolyte is preheated. The electrolyte is NaOH 30% wt.

5.3.2 Quality at different machining voltages machined during a fixed time

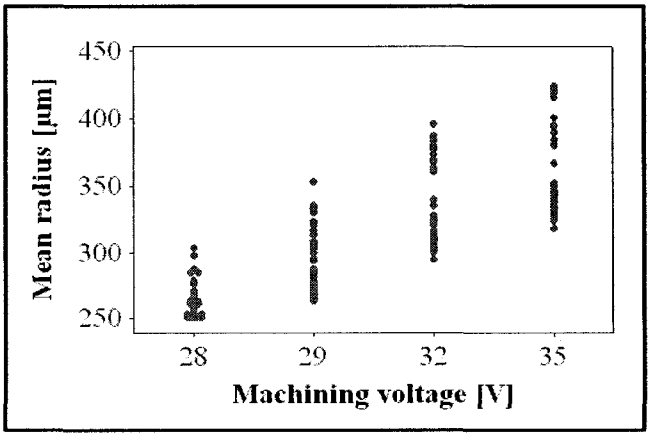

Figure 35: Interval plot of mean texture for machining voltages of 28V, 29V, 32V and 35V machined during 60s.

Figure 35 shows that the mean radius of the fitted ellipse increases as the machining voltage increases. The least variability of elliptic mean radius is detected with machining at 28V. This is possibly caused because the lower the voltage, the lower the variability is in the discharge activity [11]. Another possibility is that, the more thermal energy (due to increase of voltage) is available for machining, the higher the temperature of the tool-electrode is. AS well we can relay this on the fact that the high machining voltage produces deeper micro-holes, in which the hydrodynamic regime occurs. The shortage of electrolyte at this cases causes the discharges to occur at positions of contact which might no necessary be the tip of the electrode. Such discharges are not desirable because they yield to thermal cracks which contribute in increasing the mean radius of the micro-hole.

The variability of texture (figure 36-right) follows this pattern as well. It is worth mentioning that some other shape metrics are tested for experimental purposes and showed identical results. Some of those metrics are non-linear eccentricity and linear eccentricity of the elliptic fitting. Figure 36-left shows the interaction between the linear eccentricity and voltage, which is identical with the relationship between the mean radius and machining voltage of the sample.

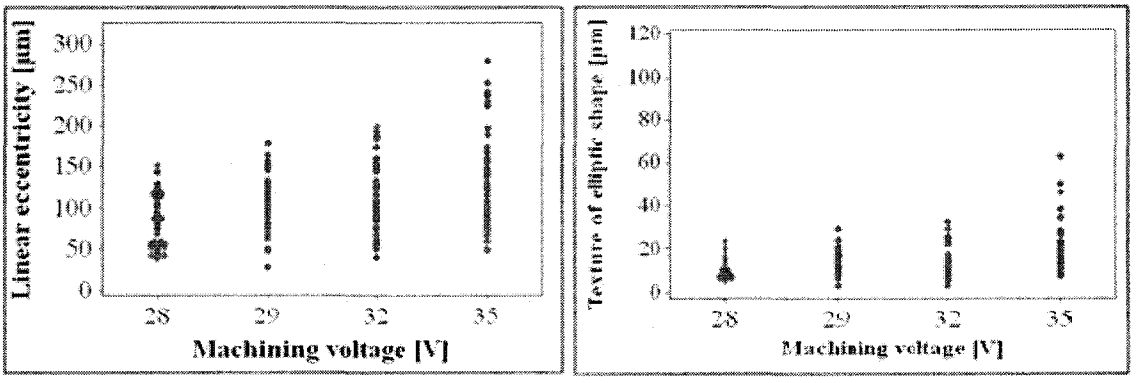

Figure 36: Interval plot of linear eccentricity (left) and texture of elliptic shape (right) with the machining voltages at machining voltages of 28V, 29V, 32V, 35V machined during 60s.

5.3.3 Variability of the traditional process

Figure 37 shows the evaluation of the micro-hole quality for a set of 50 micro-holes drilled using the traditional procedures descried in section 5.3.1. The machining voltage is 29 V and the tool electrode is a cylindrical 0.5 mm diameter of stainless steel 316L. Recognizable variability is observed in both the shape factor and texture. On the other hand the run chart of the mean radius shows an interesting pattern. For the first ten micro-holes, the mean radius is much higher than the average of the other readings. It is known that at the first ten micro-holes the machining is not repeatable, which one of the disadvantages of the traditional process, as discussed in section 2.1.9.

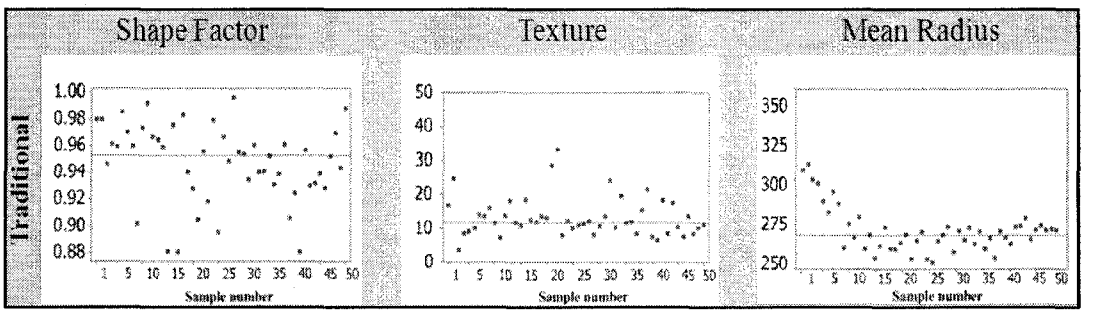

Figure 37: The quality evaluation of the traditional process. Run charts of shape factor, texture and mean radius for set of 50 micro-holes drilled with the traditional procedures. The condition of the machining is listed in section 5.3.1. The machining voltage is constant 29V DC.

5.3.4 Traditional process capability

The capability of the traditional process is calculated. The texture and the shape factor are used as a metric (figure 38). The shape factor is close to the chosen target of 95%. However the texture is slightly away from the chosen target of 12.5 μm. The spread of values for both the texture and the shape factor should be reduced, or alternatively the variability should be reduced.

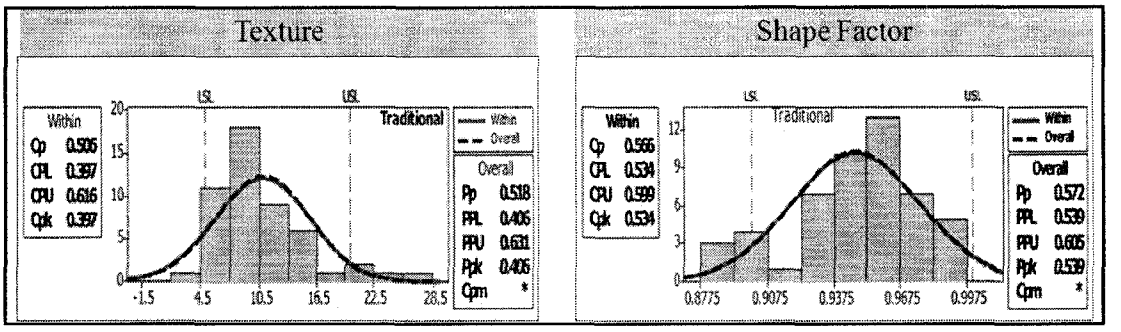

Figure 38: Capability plots of the texture and the shape factor for the tradition process. The condition of the machining is listed in section 5.3.1. The machining voltage is constant 29V DC.

5.4. Quality after improvements

5.4.1 Improved machining conditions

This evaluation is performed after the improvement procedures are introduced. Seven sets are drilled until a determined depth is reached. The voltage chosen is a DC voltage of 29 V and pulse voltage at 29 V . The tool electrode is a stainless steel 316 L and tungsten 0.5 mm cylinder. Six sets of 50 holes are drilled during variable times to reach the required depths of 50 µm, 100 µm and 150 µm. The tool electrode is initially preheated by performing free electrochemical discharges at 35 V for 5 mins before the drilling starts. The electrolyte initial temperature is set to 80 °C. The electrolyte is NaOH 30% wt. additionally one set of 50 micro-hole is drilled at a depth of 50 µm.

5.4.2 Quality of micro-holes at fixed depth and variable machining time

Figure 39 shows the shape factor versus drilling time plot for three sample of stainless steel drilled at different depths. As the depth of micro-hole increases the quality of the micro-holes tends to be more variable and further away from the target. On the other hand, the shape factor of the micro-holes of 50 µm varies between 92% and 99 %. This observation is promising and shows the importance of the implemented improvement. The standard machining process shows variability between 82% and 95%. Moreover figure 37 shows no clear interaction between the time of machining and the quality.

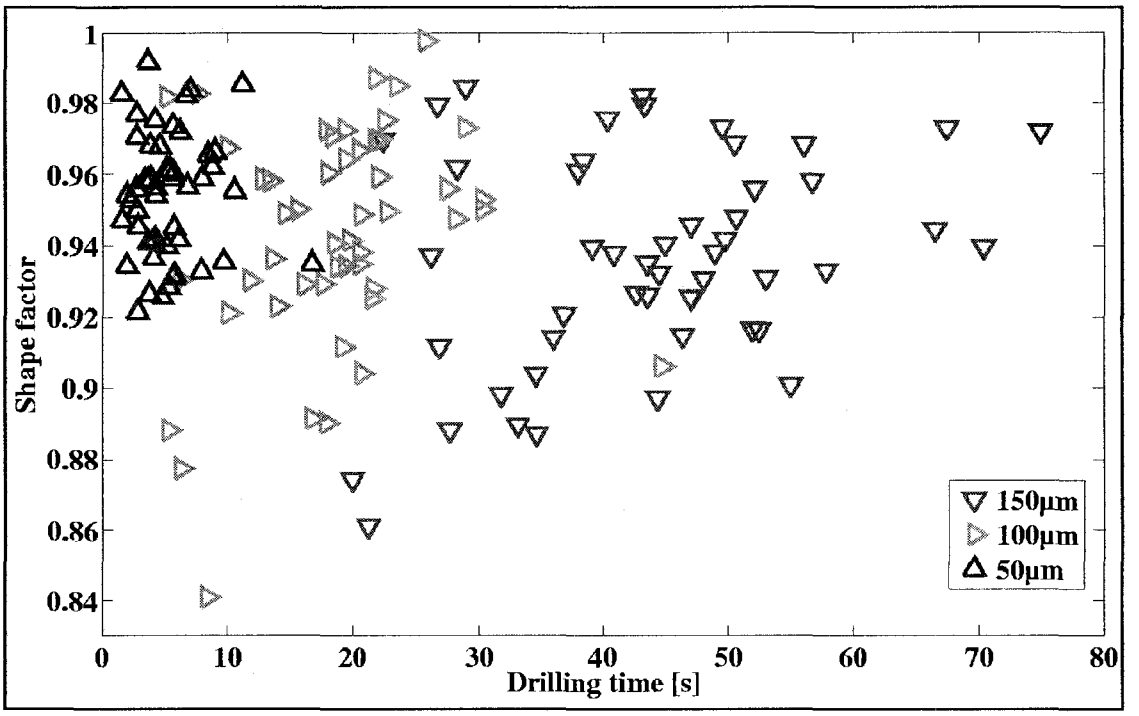

Figure 39: Shape factor versus machining time for 3 sets of micro-holes machined at different depths. The variability of shape factor increases with increasing the depth.

On the other hand, a strong dependency is noticed between the time of machining and the electrolyte level (figure 40) is noticed. This relationship agrees with observations of section 4.4 and magnifies the significance of this factor. The machining time is reduced to equal an average of 15 seconds when a very small amount of electrolyte is used. In this case, a droplet of electrolyte is added prior to the drilling on the top of the dry work-piece.

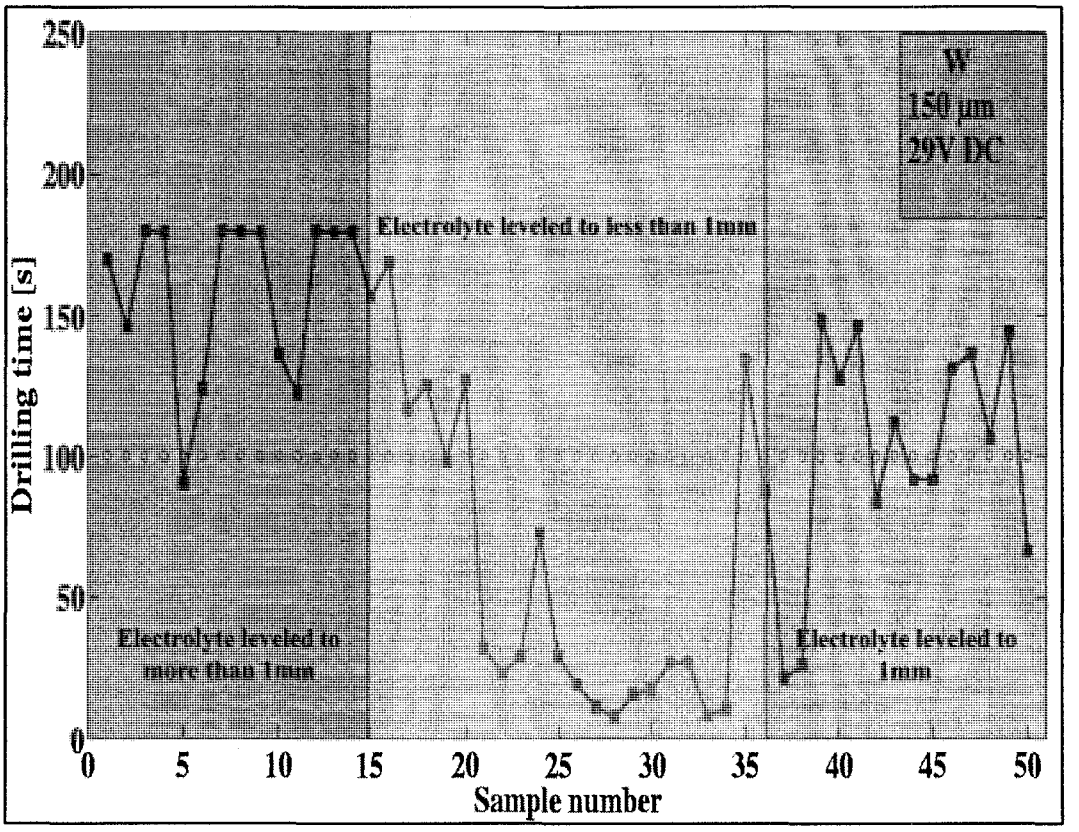

Figure 40: Run chart of drilling time in the case of drilling a micro-hole of fixed depth of 150µm at 29V. The electrode is 0.5mm of tungsten. The tool electrode is not initially preheated, and the electrolyte is preheated to 80 °C.

5.4.3 Quality of machining with pulse voltage without electrolyte adjustment

Figure 41 shows a comparison between the shape factor of micro-hole quality when machining at a fixed depth of 50 µm and the shape factor of other micro-holes drilled at the similar fixed depth. The tool electrode is a cylindrical shaped stainless steel 316 L, which preheated initially before the drilling starts. Significant variability is detected in the case of drilling at pulse voltage. This might be caused because of the lack of adjustment of low-level electrolyte and a formation of bubbles instead of gas films. The electrolyte level should be adjusted in order to reduce the variability in both machining quality and machining time.

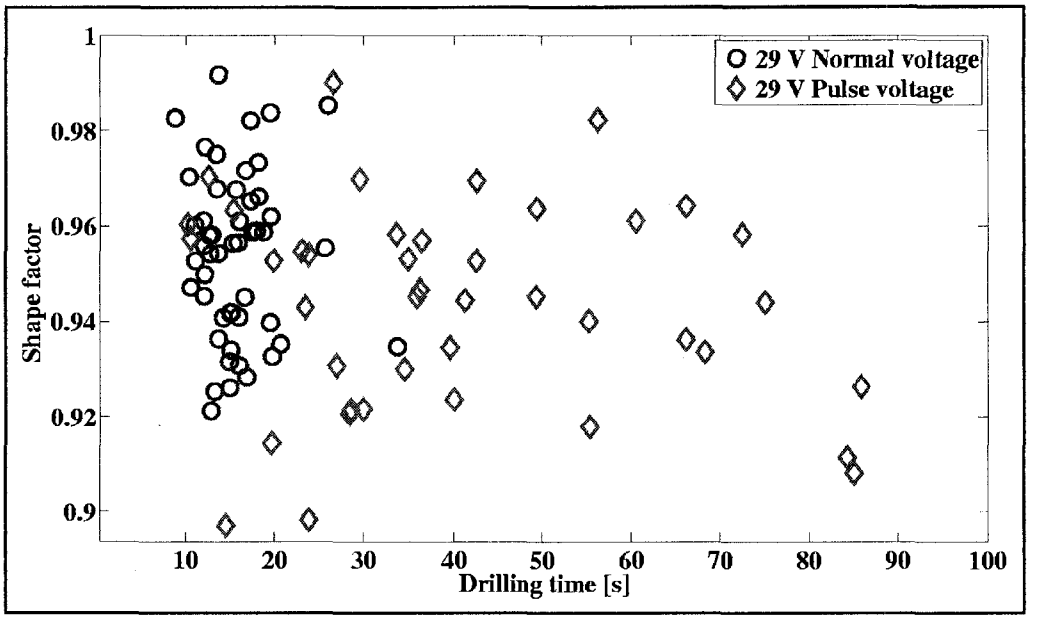

Figure 41: Shape factor versus machining time for two sets of micro-holes machined one with is machined using DC voltage and the other is machined using pulse voltage. The variability of pulse voltage drills is more significant. Drilling depth is 50μm.

5.4.4 Preheating the tool electrode

This procedure is demonstrated to reduce the non-machining status. Figure 42 shows two examples of micro-holes, one drilled without preheating the electrode and the other one with preheating the electrolyte. The electrolyte is NaOH 30% wt. initially at room temperature. The electrode is stainless steel 316 L of 0.5 mm in diameter. No significant difference in quality is observed. However the preheating of electrode is demonstrated to decrease the non-machining duration.

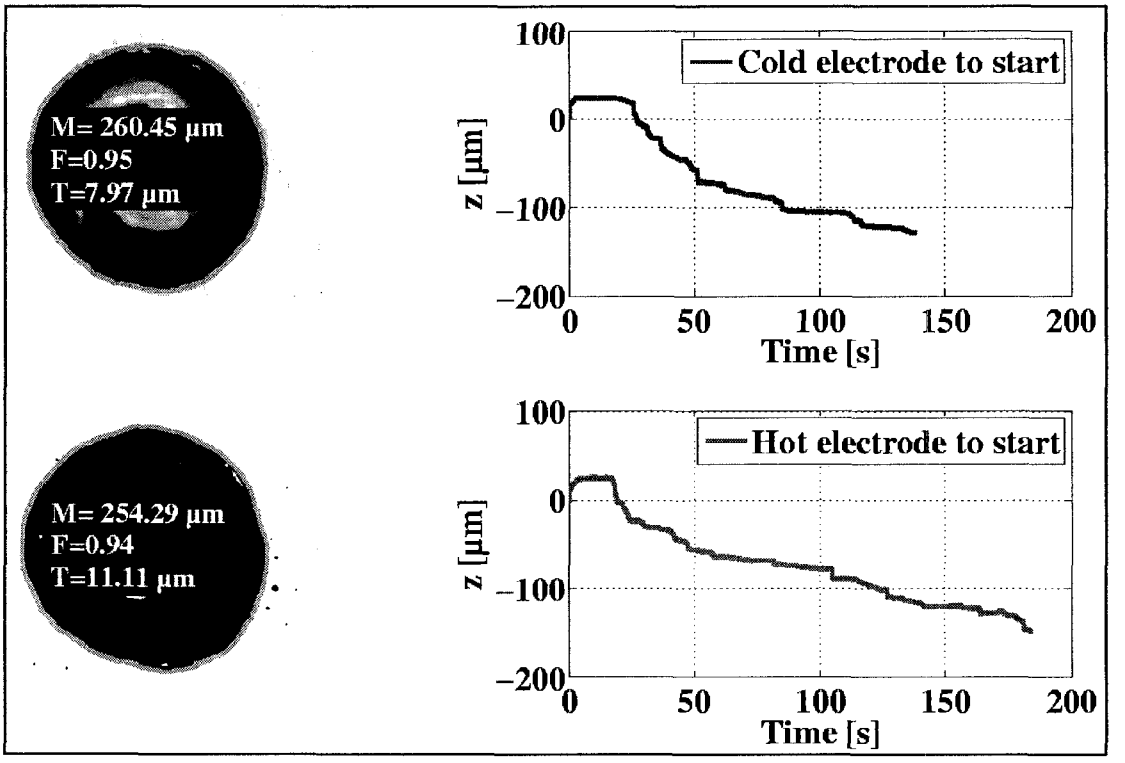

Figure 42: The effect of preheating the tool electrode. The non-machining duration time is reduced. No significant change in quality is detected.

5.4.5 Preheating the electrolyte

Heating up the electrolyte consumes some energy during the process, so that if the electrolyte initial temperature is preheated to about $60 - 80°C$ the machining removal rate will be improved (figure 43) as discussed previously in section 4.4.

The quality of micro-holes drilled with preheated electrolyte and those drilled with cold electrolyte at start (room temperature) is not investigated in this thesis.

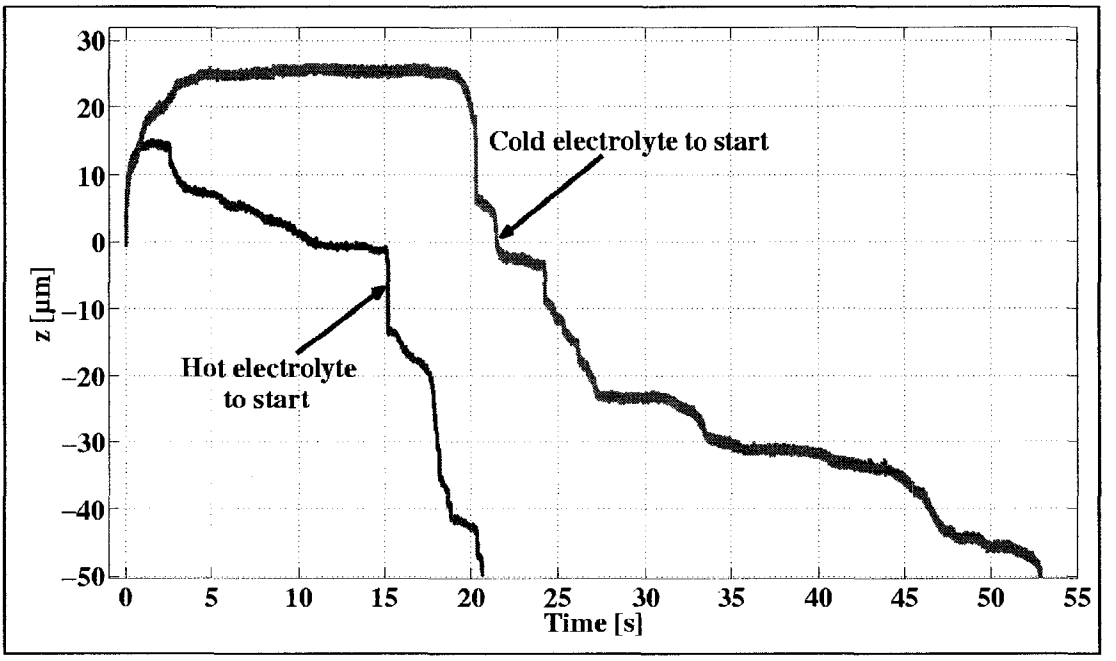

Figure 43: Evolution plots of two micro-drilling one is drilled with 80°C electrolyte and the other one is drilled without preheating the electrolyte (room temperature). Machining voltage is 29 V and electrode is preheated before the start of the drilling, and it is 0.5 mm diameter stainless steel. The micro-hole depth is 50µm.

5.4.6 Variability of the micro-hole quality with the improved process

Figure 44 shows the run charts for shape factor, texture, and mean radius for both the traditional and the improved process. It is obvious that the improved procedures yield to reducing the variability in the process.

The trend of non-repeatability occurred in the mean radius plot is now eliminated in the improved process. Such trend of non-repeatability could be caused because the tool electrode is not-preheated and it takes some time to reach some temperature. The electrolyte is not preheated at the machining as well. In the first ten micro-holes, it looks like more heat transfers through the tool electrode instead of being used in the machining. Less depth is drilled and the gas film shape is not well cylindrical, which makes the over-cut more superior in this case. This is not the case if the preheating of both the electrode and electrolyte takes place.

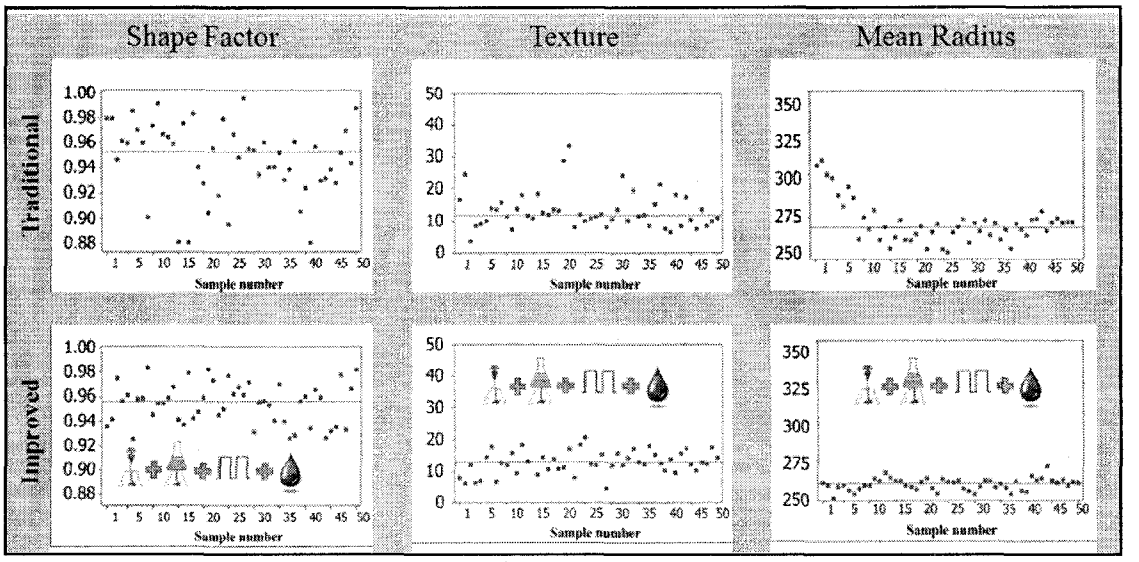

Figure 44: The quality evaluation of the traditional and improved processes. Run charts of shape factor, texture and mean radius for set of 50 micro-holes. Both the traditional and the improved processes use the same setup, however in case of the improved process the electrode and electrolyte is initially preheated, manual adjustment of the electrolyte is performed and the pulse voltage with 29V is used.

5.4.7 Capability of the improved process

Figure 45 shows the texture and shape factor capability plots. The texture capability index (Cpk) is increased from 0.397 for the traditional process to 0.724 for the improved process, as a result of reducing the variability. Similarly the shape factor capability index increased from 0.534 for the traditional process to 0.960 for the improved process. Both the process texture and shape factor are now more close to the target and show less spread around the target.

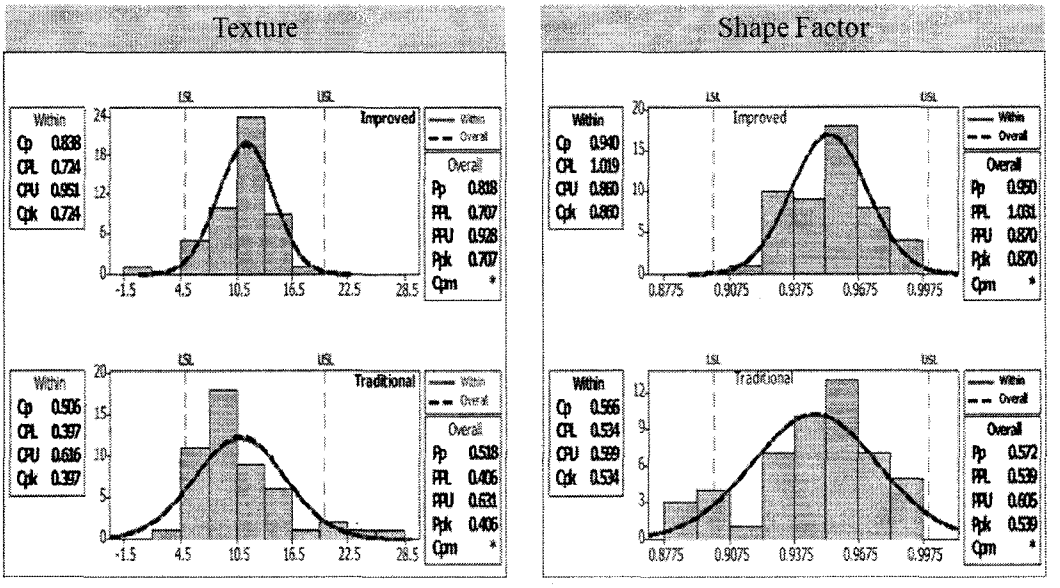

Figure 45: Capability plots of texture and shape factor for the improved process and the traditional process. Both the traditional and the improved processes use the same setup, however in case of the improved process the electrode and electrolyte is initially preheated, manual adjustment of the electrolyte is performed and the pulse voltage with 29V is used.

5.5. Quality of machining with tungsten electrodes

Figure 46 shows the quality and evolution plots and quality of two micro-holes. The machining voltage is 29 V . The electrode is a tungsten cylinder with 0.5 mm in diameter. The electrolyte is NaOH 30% wt. preheated to 80 °C . A very good quality of micro-holes could be achieved by tungsten electrodes as well, mainly at lower voltages and lower depths. Looking at figure 43, one can predict the quality from the evolution curve. Flat evolution (sample 1) caused by the shortage of the electrolyte causes the non- circularity in the micro-hole (shape factor equals 93%) for this micro-hole. However, smooth drilling in sample 2 yields to a circular (shape factor equals 99%) micro-hole.

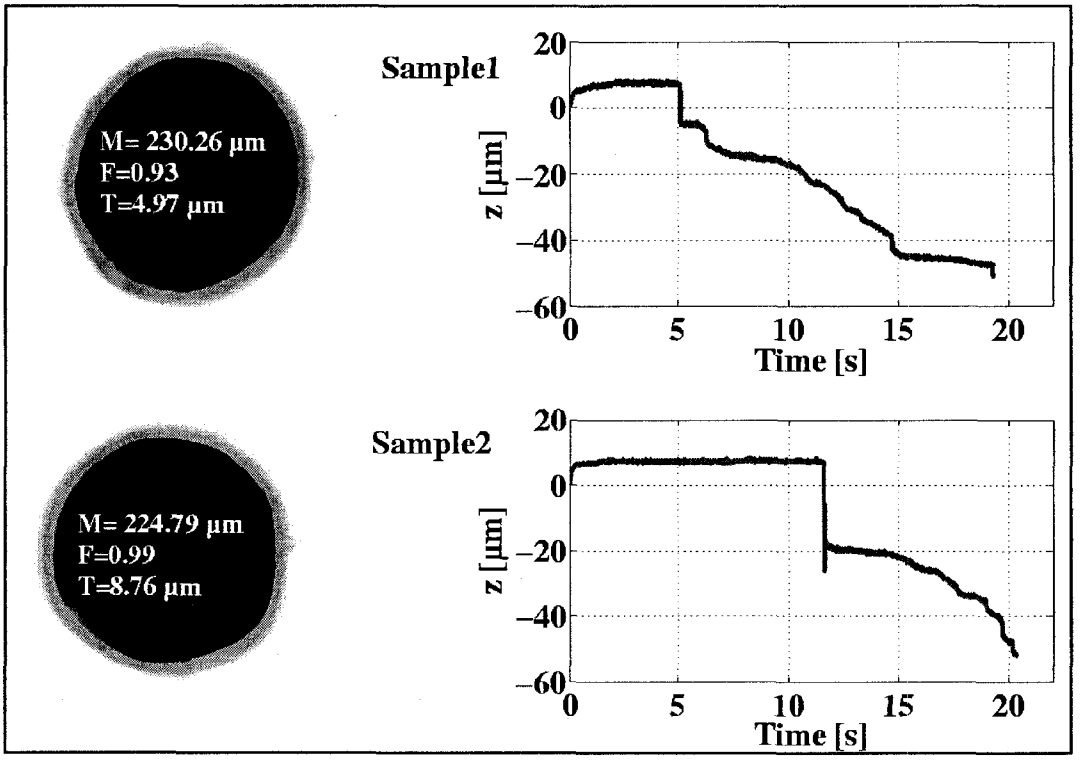

Figure 46: Two micro-holes, one with less texturing (upper-left) and another one with better shape factor (lower-left) and the corresponding evolution plot of them (right).

5.6. Summary

This chapter studied the quality of the micro-holes at different machining conditions. The metrics of the quality measures are introduced. The quality of the traditional GFMD process with machining during 60 s is examined. The capability is used to evaluate the process at that stage. However after implementation of preheating the electrode and preheating the electrolyte and applying pulse voltage with manual adjustment of the electrolyte level, drilling to 150µm fixed depth another quality evaluation is performed. The capability of the process is doubled after the improvement. The improved procedures drive the process to be centred more around the target with less variability. Drilling deep micro-holes requires more investigation to the electrolyte levelling issue and even to the electrolyte delivery as well.

Chapter 6
Conclusion

6.1. Concluding remarks

In this thesis, experimental investigation and theoretical evaluation of the GFMD process is carried out. The idea behind this study is to incorporate the quality of the micro-holes and the machining time with process assessment to improve the GFMD.

To formulate a strategy for improvement, this study examines different process factors and analyzes their effect on the process through statistical process control tools such as run chart, cause and effect diagrams, interval plots and capability analysis.

These tools are proven to be useful and led to a preliminary improvement on the micro-drilling with GFMD. They could in particular reveal a new assignable cause, not yet identified so far, the electrolyte level.

In this investigation the heat transfer and chemical contribution are believed to have a significant effect on the quality and the machining time.

The thermal conductivity and the discharge activity of tool electrode material determine the amount of thermal energy lost trough the electrode. The use of geometry metrics combined with evolution data provided quantitative measures of the overall process.

Implementing some procedures such as preheating the electrode, preheating the electrolyte and the use of pulse voltage enhanced the capability in the positive direction. This indicates that our changes are useful.

The evident relation between the evolution and the quality makes this study introduce this signal as a real-time sensing signal of the process. Future control mechanisms shall use the interpretation of this signal as well as the current signal for close-loop controllers.

6.2. Recommended improvements for future work

Based on the results of this investigation the following improvements for the process are proposed for future work:

6.2.1 To implement electrolyte leveling system

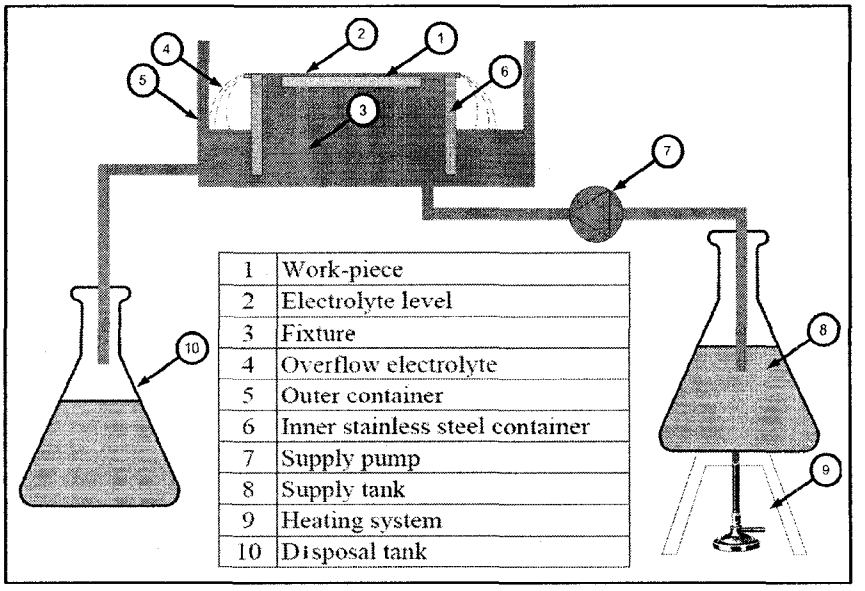

Figure 47: Schematic of electrolyte levelling technique.

The electrolyte levelling system (figure 47) that is suggested in section 4.4 is most likely capable of eliminating the variability that occurs due to changing the level during the machining. It is worth mentioning that change of surface tension due to applying the machining voltage might be an obstruction to adjust very low levels of electrolyte. Moreover it is suggested to investigate the electrolyte feeding mechanism (figure 27) with a syringe pump and a hollow electrode (figure 48).This might help in providing the electrolyte into the machining area, to promote the chemical etching and avoid the slowdown in machining due to the shortage of electrolyte.

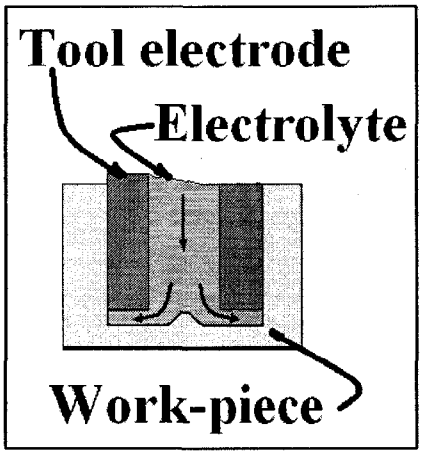

Figure 48: Cross-section of electrolyte injecting tool. The electrolyte is dispensed internally to the machining zone to overcome the shortage throughout the drilling.

6.2.2 To implement tool electrode orbital motion

Although orbital motion was investigated for similar machining techniques, this is not yet implemented in GFMD. Such improvement might lead to well cylindrical micro-holes. This could by either using cylindrical tool electrode or by using helical tool (figure 49). While rotating the helical tool might feed electrolyte into the micro-hole during the drilling and at the same time might improve the evacuation of the melted zone. The effect of the helical shaped tool on the material removal rate and the quality of the micro-holes might be an interesting subject of the study.

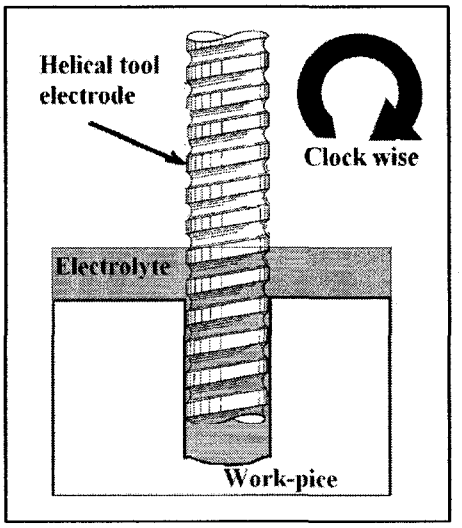

Figure 49: Helical tool electrode, to feed electrolyte into the machining zone to improve the chemical etching and to evacuate the melted material.

6.2.3 Synchronizing the tool vibration pulse voltage and the dispensing

The significant drawback noticed in machining with pulse voltage that it is dependable extensively on the electrolyte. Hence a vibratory motion is applied during the machining with pulse voltage and combining both with electrolyte dispensing (figure 50). It is presumed that this might significantly improve the quality of the micro-holes, due to the promotion of chemical etching and at the same time it might improve the material removal rate which is known to be improved when the tool electrode vibration is applied.

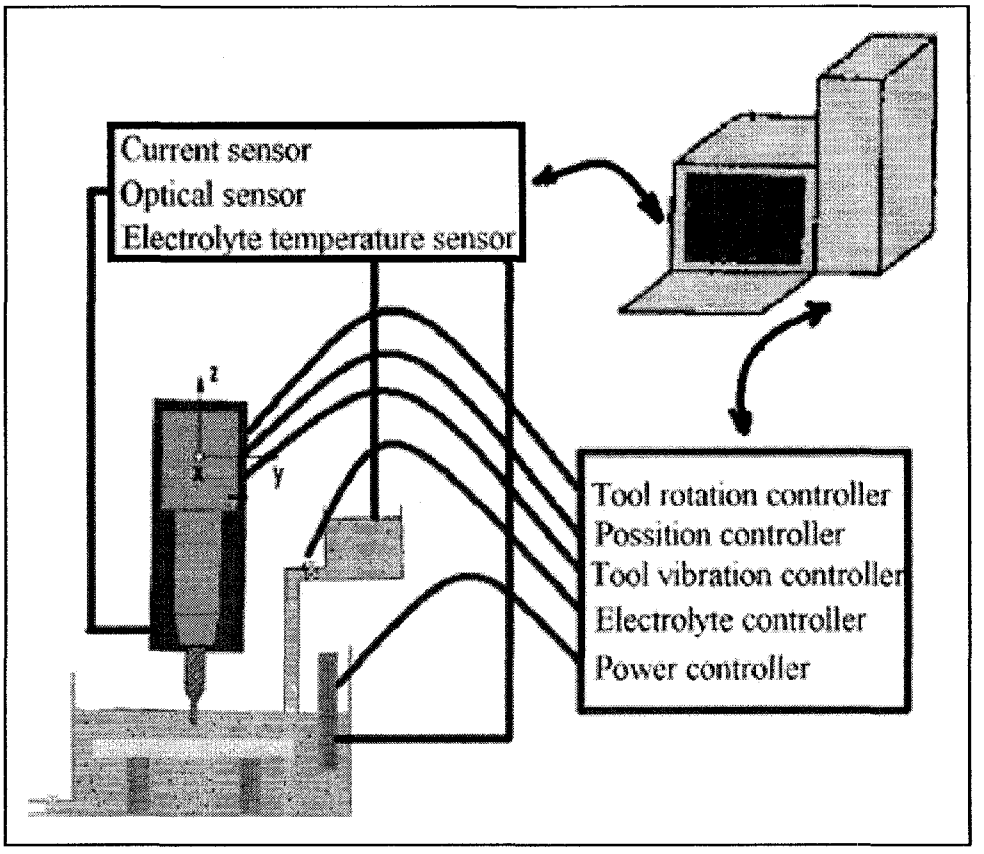

Figure 50: Sketch of overall control system for GFMD. The vibration, pulse voltage and electrolyte feeding is synchronized.

6.2.4 Investigating the overall geometry of the micro-hole

Studying only the entrance surface of the micro-hole might not be enough to characterize the quality of such micro-hole. It might be interesting to investigate the overall geometry of the micro-hole. New measures and rather more significant metrics could be presented. The cylindricity, concentricity, circular run-out, and total run-out might contribute in detecting one or more deficiencies in the machining .

6.2.5 Using stair-case-like evolution for predicting quality and machining time

The importance of studying the stair case evolution comes from the shortage of prediction metrics in GFMD. This might increase our knowledge about the process itself. So far the current signal is

known to identify and predict the information that this evolution. A prediction model that can link the characteristics of stair case evolution with the quality and the material removal rate could be a major innovation in the GFMD.

6.3. Contribution to knowledge

Throughout the thesis was stressed that the GFMD has a potential for improvement, which are necessary to become competitive with other micro-drilling processes. It was the main goal of the study to lay the strategy and direction for improvement through statistical control tools. The methodology and experimental observations gathered in this thesis can now be readily saved to further improve and evaluate the process. The results obtained along with the proposed future work form the conclusion shall prove useful in designing more complex GFMD- like processes in the field of micro-drilling.

References

[1] Wüthrich R and Fascio V 2005 Machining of non-conductive materials using electrochemical discharges phenomenon—an overview. *Int. J. of Mach Tools Manuf.* 45 1095-108

[2] Kurafuji H and Suda K 1968 Electrical discharge drilling of glass. *Ann. CIRP* 16 415–9

[3] Wüthrich R, Spaelter U, Wu Y, Bleuler H 2006 A systematic characterization method for gravity-feed micro-hole drilling in glass with Spark Assisted Chemical Engraving (SACE). *J. Micromech. Microeng.* 16 1891-1896

[4] Wüthrich R, Spaetler U, Bleuler H, 2006 The current signal in Spark Assisted Chemical Engraving (SACE), what does it tell us ?. *J. Micromech. Microeng.*16 779-785

[5] Gautam N and Jain V K 1998 Experimental investigations into ECSD process using various tool kinematics. *Int. J. Mach. Tools Manuf.* 38 15–2

[6] Wüthrich R, Despont B, Maillard P, Bleuler H 2006 Improving drilling speed in Spark Assisted Chemical Engraving (SACE) by tool vibration. *J. Micromech. Microeng.*16 28-31

[7] Wüthrich R, Fujisaki K, Couthy Ph, Hof L A and Bleuler H 2005 Spark assisted chemical engraving (SACE) in microfactory. *J. Micromech. Microeng.*

[8] Maillard P 2007 *Investigation on material removal process in SACE glass machining design of a force measuring set-up.* Master thesis, Swiss Federal Institute of Technology, EPF Lausanne

[9] Jalali M, Maillard P, Mishra S P, Kadem L, Wüthrich R 2007 Modelling gravity feed micro hole drilling by electrochemical discharge. *2nd Int. Conf. on Micro-Manufacturing*, Greenville, South Carolina, USA

[10] Kim D-J, Ahn Y, Lee S-H, Kim Y-K (2006) Voltage pulse frequency and duty ratio effects in a electrochemical discharge micro-drilling process of Pyrex glass. *Int. J. of Mach. Tools and Manuf.* 46 p. 1064

[11] Wüthrich R (2007) *Fundamentals and Application of Spark Assisted Chemical Engraving.* William Andrew Micro & Nano Technologies (MNT) Series (under-press).

[12] Zheng Z-P, Cheng W-H, Huang F-, Yan Y B-H (2007) 3D microstructuring of Pyrex glass using the electrochemical discharge machining process. *J. Micromech. Microeng.*17 p. 960

[13] West J, Jadhav A (2007) ECDM methods for fluidic interfacing through thin glass substrates and the formation of spherical microcavities. *J. Micromech. Microeng* 17 403-409

[14] Jain V K, Rao P S , Choudhury S K , Rajurkar K P (1991) Experimental investigations into travelling wire electrocheimical spark machining (TW-ECSM) of composites Trans. ASME. *Journal of Engineering for Industry* 113 p. 75

[15] Zheng Z-P, Su H-C, Huang F-Y, Yan B-H (2007) The tool geometrical shape and pulse-off time of pulse voltage effects in a Pyrex glass electrochemical discharge micro-drilling process Journal of Micromechanics and Microengineering 17 p. 265

[16] Jain V K, Choudhury S K, Ramesh K M (2002) On the machining of alumina and glass. *Int. J. of Mach. Tools and Manuf.* 42 p. 1269 -1276.

[17] Maillard P, Despont B, Bleuler H, Wüthrich R (2007) Geometrical characterization of micro-holes drilled in glass by gravity-feed with spark assisted chemical engraving (SACE). *J. Micro-mech. Microeng* 17 1343-1349

[18] Oakland, J S (2003) *Statistical Process Control* Butterworth-Heinemann fifth edition

[19] Deming W E (1986) *Out of the Crisis.* MIT Centre for Advanced Engineering Study, Cambridge, Massachusetts.

[20] Wüthrich R, Hof L (2006) The gas film in spark assisted chemical engraving (SACE) - A key element for micro-machining applications. *Int. J. of Mach. Tools and Manuf.* 46 p.828

[21] Box, G E P, Hunter W G, Hunter J S (1978) *Statistics for Experimenters* Wiley-Inter science

[22] Sarkar B R, Doloi B, Bhattacharyya B (2006) Parametric analysis on electrochemical discharge machining of silicon nitride ceramics. *International Journal of Advanced Manufacturing Technology* 28 p.873-881

[23] http://www.mathworks.com/matlabcentral/files/15125/content/demo/html/ellipsedemo.html

[24] Thoe T B , Aspinwall D K , Wise M L H (1998) Review on ultrasonic machining. *Int. J. of Mach. Tools and Manuf.* 38 p. 239-255

[25] Yerokhin A L, Nie X, Leyland A, Maetthews A, Dowey S.J. (1999) Plasma electrolysis for surface engineering. *Surf. Coat. Tech.* 122 73–93

[26] Reghuram V (1994) *Electrical and spectroscopic investigations in electrochemical discharge machining* Dissertation Thesis, Indian Institute of Technology, Madras and Indian Institute of Technology, Kanpur

[27] Raghuram V, Pramila T, Srinivasa Y G, Narayanasamy K (1995) Effect of the circuit parameters on the electrolytes in the electrochemical discharge phenomenon. *Journal of Material Possessing Technologies* 52 301–318

Appendices

Appendix A

A.1. Cost analysis

Although the GFMD and SACE in general are simple and costly, this thesis presents an introduction to the cost analysis as cause and effect diagram (figure 51) shows the possible cause of increasing the cost if research and development set up is used as a production process.

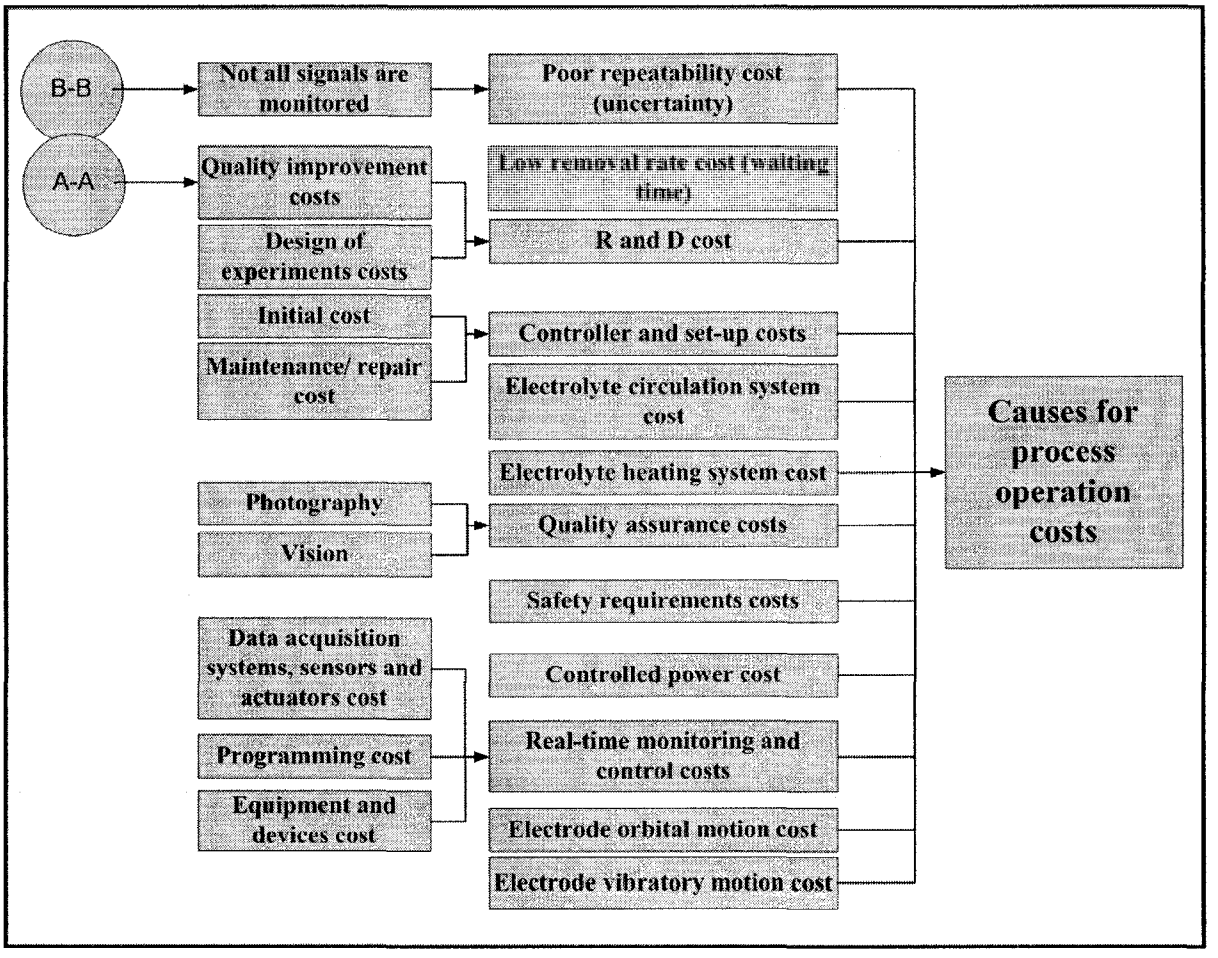

Figure 51: Cause and effect diagram of the process operational cost, if the research and development setup is used as a production setup for GFMD. A-A and B-B are described in figure 5 and figure 10.

A.2. Significant root causes

After the root causes are determined using the cause and effect diagrams, a study of ordering those causes from the most significant ones to the least significant ones should be carried out. Focus groups and customer surveys are good tools to collect such information. The customer's opinion is giving this information indirectly. The information collected by those surveys should be analyzed by an expert with the process interactions. Looking to figure 52, one can observe three major root causes, which are:

- Electrolyte level variability
- Gas film instability
- Non-machining status

Other minor root causes can be left to the further stages of the improvement.

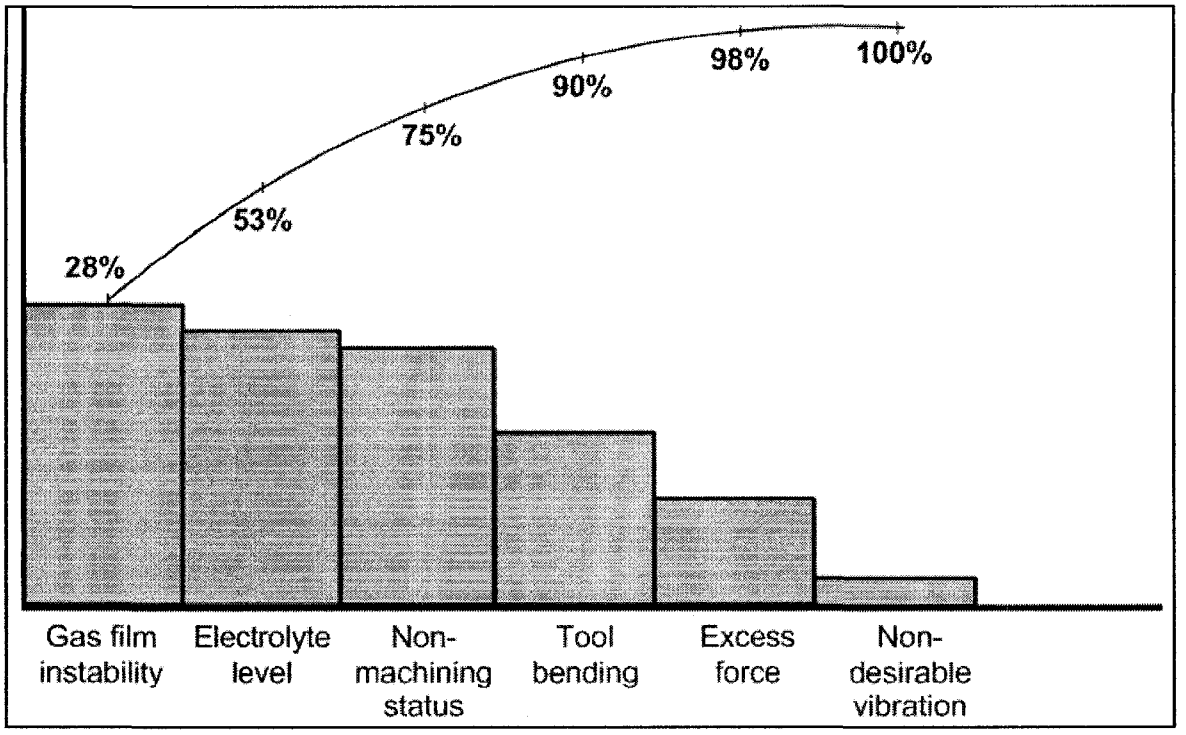

Figure 52: Pareto diagram of the major error states. The data is collected by an error frequency survey.

Appendix B

B.1. Micro-hole edge tracking

This vision system is programmed using Matlab image processing tool box. The flowchart in figure 53 shows the procedure of the vision system. The contour that follows upper surface edge of the micro-holes is determined, as a matrix of X and Y axis coordinates. These coordinates are used in calculating the mean radius, the shape factor and the texture.

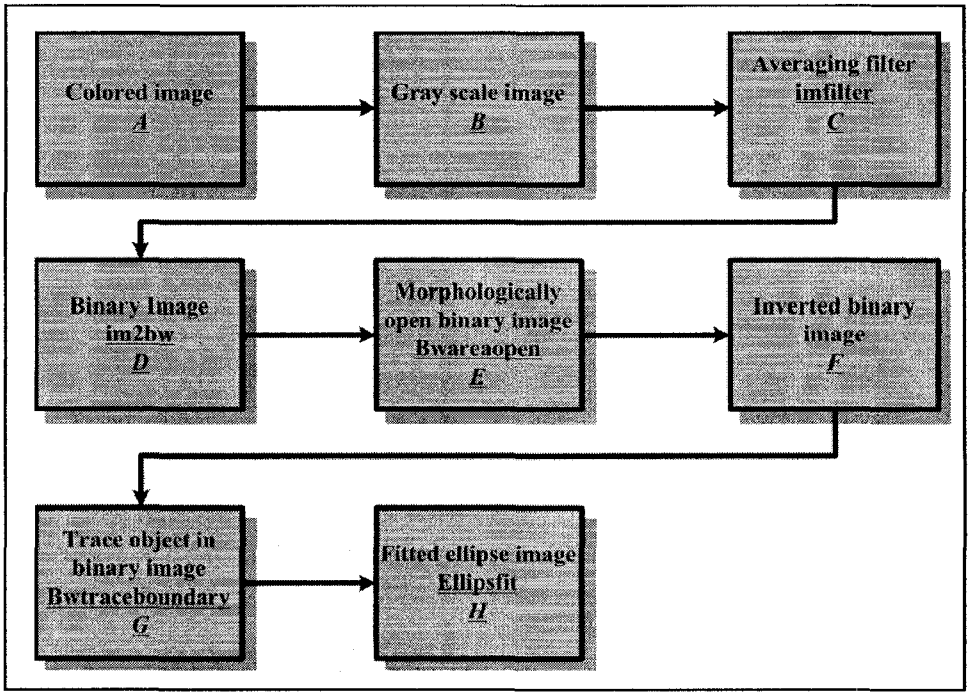

Figure 53: The flow chart of the Micro-hole edge tracking vision system.

Figure 54 shows the output of each step of the vision system. The processing of each 20 micro-images takes around 60 seconds in case of no image display.

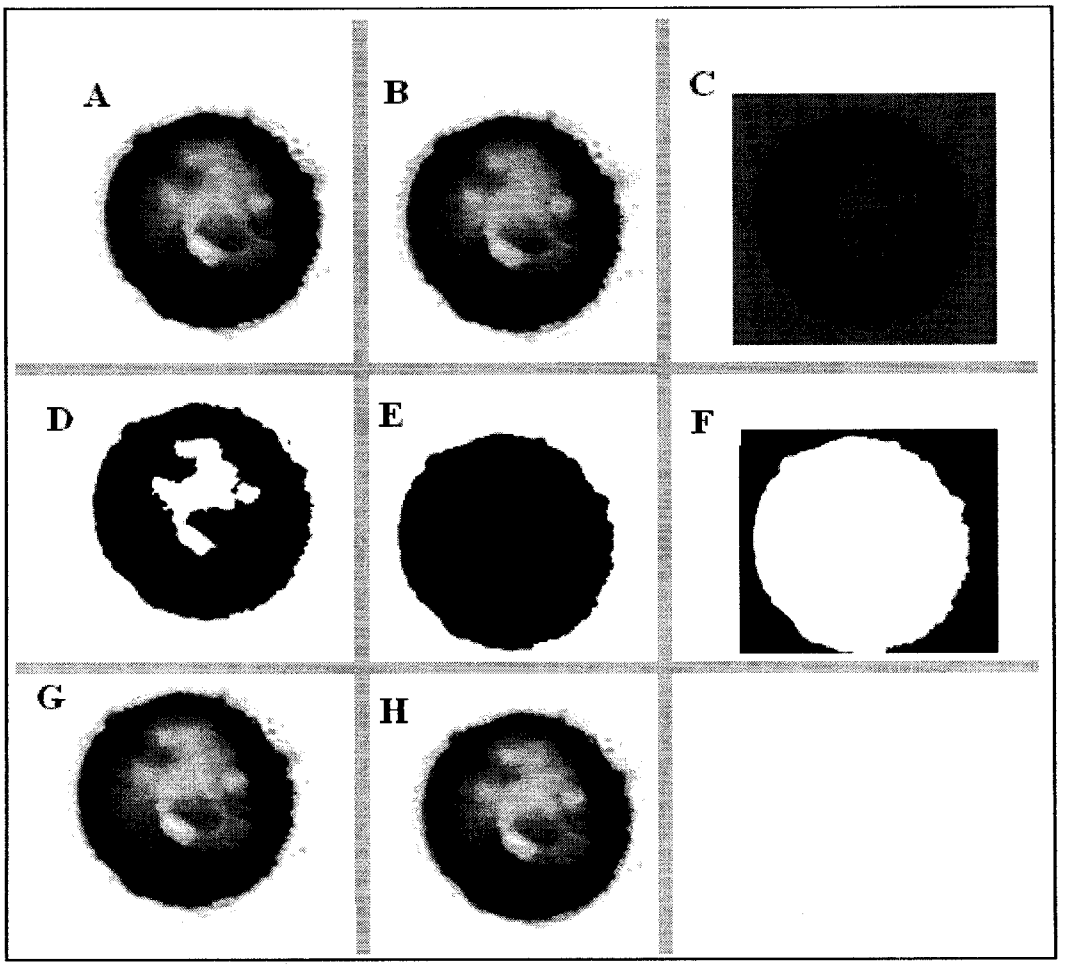

Figure 54: The output of each step in the vision system.

Appendix C

C.1. Pulse voltage circuit

To minimize the instability in the gas film, which affects the repeatability of machining, the pulse voltage circuit is introduced. Figure 55 shows the implementation of the RL Circuit and its effect on the current signal when connecting to the machining cell. When the critical current is reached the gas film is fully developed, and acts as a capacitor. This blocks the current causing the discharges to occur, for very short time. Then the current increases as the gas films grow up again until reaching the critical current again the phenomenon is repeated again and again.

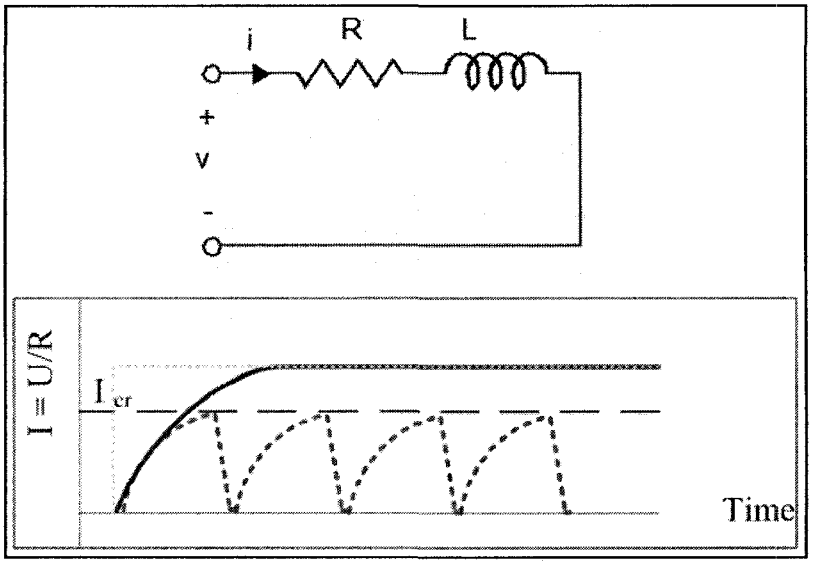

Figure 55: The ideal current signal from RL circuit (solid line) and the expected current response when connecting to the machining cell (hidden line).

C.2. Electrolyte level interpretation

When the tool electrode is immersed in the electrolyte, the interfacing surface between the tool electrode the electrolyte is represented as follows (in case of cylindrical electrode):

$$S = \pi r'^2 + 2\pi r'L \qquad (8)$$

S : is interfacing surface [μm^2]

r′ : is radius of electrode [μm]

L : is level of the electrolyte [μm]

The increase in the electrolyte level yields to an increase in the critical current, which makes the gas film formation takes shorter times in case of lower levels. The electrolyte level can be measured by the current signal of the cell. The lower the level, the higher the magnitude of the current signal shall be. A plot of critical current as a function of electrolyte level is shown in figure 56.

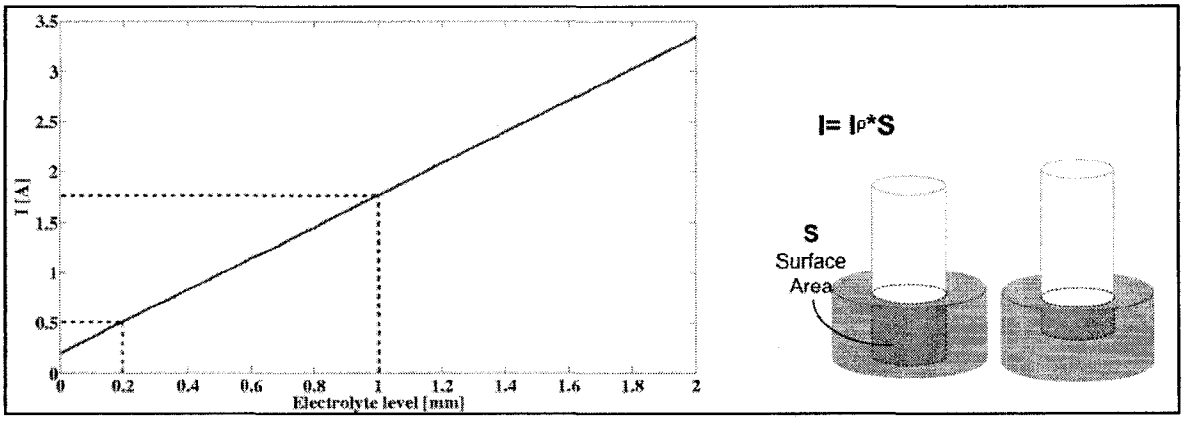

Figure 56: Interpreting the electrolyte level as the interfacing area between the electrode and electrolyte. Iρ is the current density of the cell, and S is the total interfacing area. The tool electrode is 0.5 mm in diameter and the current density is $1.0\ \frac{A}{mm^2}$.